SANDIA REPORT

SAND99-2168
Unlimited Release
Printed August 1999

A Numerical Feasibility Study of Three-Component Induction Logging for Three Dimensional Imaging About a Single Borehole

David L. Alumbaugh and Michael J. Wilt

Prepared by
Sandia National Laboratories
Albuquerque, New Mexico 87185 and Livermore, California 94550

Sandia is a multiprogram laboratory operated by Sandia Corporation, a Lockheed Martin Company, for the United States Department of Energy under Contract DE-AC04-94AL85000.

Sandia National Laboratories

Issued by Sandia National Laboratories, operated for the United States Department of Energy by Sandia Corporation.

Available to DOE and DOE contractors from
Office of Scientific and Technical Information
P.O. Box 62
Oak Ridge, TN 37831

Prices available from (703) 605-6000
Web site: http://www.ntis.gov/ordering.htm

Available to the public from
National Technical Information Service
U.S. Department of Commerce
5285 Port Royal Rd
Springfield, VA 22161

NTIS price codes
Printed copy: A04
Microfiche copy: A01

SAND99-2168
Unlimited release
Printed August 1999

A NUMERICAL FEASIBILITY STUDY OF THREE-COMPONENT INDUCTION LOGGING FOR THREE DIMENSIONAL IMAGING ABOUT A SINGLE BOREHOLE

David L. Alumbaugh
Geophysical Technology Department
Sandia National Laboratories
PO Box 5800
Albuquerque, NM 87185-0750

Michael J. Wilt
Electromagnetic Instruments, Inc.
1301 South 46th St; Bldg. 300
Richmond Field Station
University of California
Richmond, CA 94804

ABSTRACT

A theoretical analysis has been completed for a proposed induction logging tool designed to yield data which are used to generate three dimensional images of the region surrounding a well bore. The proposed tool consists of three mutually orthogonal magnetic dipole sources and multiple 3 component magnetic field receivers offset at different distances from the source.

The initial study employs sensitivity functions which are derived by applying the Born Approximation to the integral equation that governs the magnetic fields generated by a

magnetic dipole source located within an inhomogenous medium. The analysis has shown that the standard coaxial configuration, where the magnetic moments of both the source and the receiver are aligned with the axis of the well bore, offers the greatest depth of sensitivity away from the borehole compared to any other source-receiver combination. In addition this configuration offers the best signal-to-noise characteristics. Due to the cylindrically symmetric nature of the tool sensitivity about the borehole, the data generated by this configuration can only be interpreted in terms of a two-dimensional cylindrical model. For a full 3D interpretation the two radial components of the magnetic field that are orthogonal to each other must be measured. Coil configurations where both the source and receiver are perpendicular to the tool axis can also be employed to increase resolution and provide some directional information, but they offer no true 3D information.

The sensitivity analysis has been formulated in terms of the tool induction number. If the magnetic permeability is assumed to be that of free space, the induction number reduces to the product of the frequency, the electrical conductivity of the medium, and the square of the source-receiver separation. Normalizing the results in this manner allows us to choose the appropriate frequency(s) and separation(s) at which the tool response is optimized for a given formation conductivity. In this case the optimal response occurs between an induction number of 0.1 and 10; above and below these values the signal-to-noise ratio will degenerate. In addition, below an induction number of 0.1, the tool is much more sensitive to the near borehole than to regions away from the borehole, and the ratio between the high and low sensitivities is constant with decreasing induction number. Thus decreasing the frequency such that the induction number is less than 0.1 will not provide greater depths of sensitivity.

Following the sensitivity analysis we conduct a numerical modeling study to 1) validate the sensitivity study, and 2) analyze the feasibility of three dimensional (3D) electromagnetic (EM) imaging from a single borehole. Synthetic data calculated with a finite difference scheme for a simple 3D model demonstrate that the phase of the magnetic fields perpendicular to the axis of the borehole provide the critical information about the "three dimensionality" of the medium. In addition it is demonstrated that null coupled

fields generated by a 3D body are of sufficient magnitude to be measurable in the presence of the maximum coupled field.

Because the proposed tool is composed of multiple sondes, the measured fields are prone to errors due to misalignment and rotation between the sources and receivers. A simple analysis shows that although the effect on the maximum-coupled fields is negligible, a biased error results in the null coupled fields that easily exceed 10% in amplitude and 50° in phase. Because high quality null coupled data is a necessity for 3D interpretation, accurate location of the various sensors with respect to each other is necessary.

In the final section of the analysis a 3D inversion algorithm is employed to demonstrate the plausibility of 3D imaging using three component magnetic field data. Here it is experimentally illustrated that a three component source provides better resolution than a single component source aligned parallel to the axis, and that longer source-receiver offsets allow for greater imaging depths away from the borehole.

ACKNOWLEDGEMENTS

This work was performed at Sandia National Laboratories with funding provided by ElectroMagnetic Instruments, Inc., and the Department of Energy's Office of Geothermal Technology. Sandia is a multiprogram laboratory operated by Sandia Corporation, a Lockheed Martin Company, for the United States Department of Energy under Contract DE-AC04-94AL85000.

TABLE OF CONTENTS

CHAPTER I

INTRODUCTION

Often the drilling of a well (oil, geothermal, or otherwise) is followed by a down-hole logging process to characterize the region immediately surrounding the well bore. The electromagnetic (EM) induction log, which provides an estimate of the formation's bulk electrical resistivity, is among the most frequently employed borehole characterization tools. Commercial EM induction logging tools employ a magnetic field source, usually consisting of a small solonoid, the magnetic dipole moment of which is parallel to the axis of the borehole. Measurements are then made of the axial magnetic field at offsets of 2 m or less away from the source (Figure 1a). This allows for one dimensional (1D in the direction parallel to the borehole), or under the assumption that the geology is cylindrically symmetric about the borehole, two-dimensional (2D) interpretations of the formation adjacent to the well bore. The cylindrical symmetry assumption is usually adequate for wells that are nearly vertical and are drilled through what is primarily a 1D layered sequence. These commercial tools allow for good vertical resolution due to 1) the close proximity of the source and receiver (often under 1m) and 2) the fact that all sources and sensors are located on a single rigid boom or sonde. The latter allows for differencing techniques to be applied to the data which removes the free space or primary field, and thus allows the scattered field generated by the formation to be more accurately determined within the dynamic range limitations of the measurement system. Unfortunately, because the maximum source-receiver offset is often less than 2m the tool sensitivity is limited to features that are located within at most 3 to 5 meters of the well.

In regions of complex geology, or in the case of deviated wells, it is often desirable to have directional sensitivity to off-axis structures such as fractures, formation heterogeneity, and/or bedding planes that intersect the well bore at an angle. For reasons that will be demonstrated below, standard induction logs can not provide the information required to resolve these features that do not obey a cylindrical symmetry. In addition, to delineate heterogeneity that is located further away from the borehole than can be sensed by traditional tools, larger source-receiver offsets must be employed. Thus to resolve 3D

structures at distances several to tens of meters away from the borehole, it is necessary to employ non-standard tool configurations utilizing magnetic field sensors (and/or sources) that are aligned both along the tool axis as well as perpendicular to it, and source-receiver offsets that are greater than those routinely employed. At present there are no commercial tools offering this configuration, and only one prototype three component tool has been described in the literature (Sato et al., 1993 ; Wilt and Alumbaugh, 1998).

In this report we determine which source-receiver-frequency measurement configurations are most appropriate for delineating non-cylindrically symmetric structures. To initiate this analysis we will assume a sensor arrangement as described in Figure 1b. Here the logging tool consists of a transmitter module containing three magnetic dipole sources which are orthogonal to each other, and can transmit at multiple frequencies. The primary transmitter sonde also contains at least one three component receiver, and additional receivers are mounted on secondary sondes or pods that trail the primary at various distances. Note, these secondary sondes are required for larger source-receiver separations as a single tool becomes technically unfeasible to build for separations greater than 20m or so. The sondes are then connected together by reinforced or armored logging cable. It must be stressed that we are trading off greater depth of sensitivity against resolution because as multiple sondes become necessary, the free space field can no longer be easily removed via differencing due to the effects of small changes in the orientation between the transmitter and receiver.

The study is initiated in Chapter II using a sensitivity analysis originally developed for 2D medium that is cylindrically symmetric media about a borehole tool (Moran ,1982), and later extended to 2.5D and 3D crosswell electromagnetic (EM) measurements (Spies and Habashy ,1995). This indicates not only the frequencies and separations at which the tool response is optimal, but also those regions around the borehole to which the tool is most sensitive. In Chapter III we demonstrate the practicality of making three component measurements of the magnetic fields generated by magnetic dipole sources of various orientation. The first part of the analysis will involve numerical modeling of the proposed tool response to an isolated 3D body which is located asymmetrically about the borehole. Through this analysis we will not only validate certain components of the sensitivity study,

but also demonstrate that the maximum and null coupled components of the target response are large enough to be measurable in the presence of the primary, or free space field. We also demonstrate how deviations in the borehole, and rotation between the source and receivers, can introduce biased errors within the data. Finally in Chapter IV we demonstrate through the inversion of a synthetic data set that 3D images of the region surrounding the borehole can be reconstructed, and how different measurements and/or source-receiver offsets affect the resulting image.

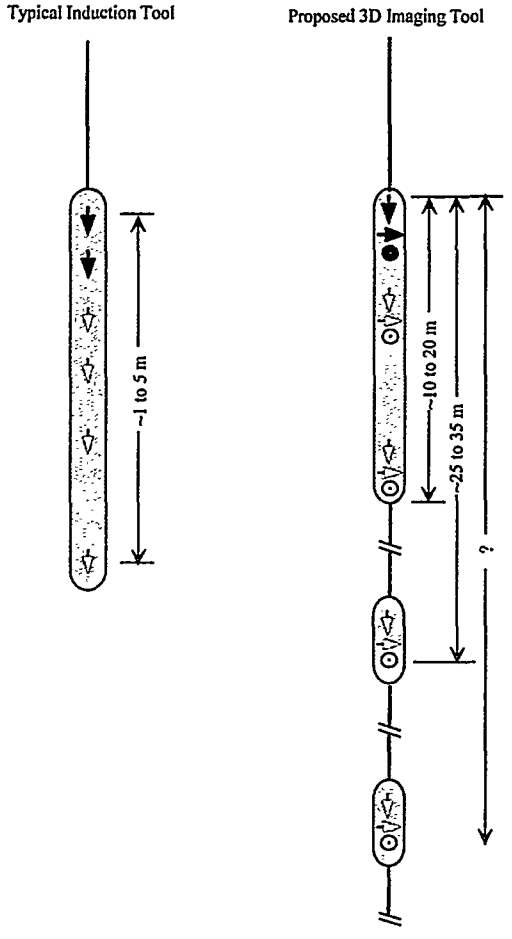

Figure 1 – a) Configuration of the standard, commercially available induction logging tool. Black arrows represent the sources, white arrows the receivers, and the direction the arrows are pointing designate the orientation of the sensors. b) Proposed 3-component log offset logging tool. Black arrows represent the sources, the white arrows the receivers, and the direction the arrows are pointing designate the orientation of the sensors. The circles represent arrows pointing out of the page.

CHAPTER II

SENSITIVITY ANALYSIS

In this sensitivity study, we wish to theoretically analyze two topics with regards to the proposed tool. The first topic of interest is to determine the combination of frequency and source-receiver separation that yields optimal measurements in terms of both the instrument signal-to-noise ratio (SNR), as well as the formation signal-to-free space field ratio, given both a realistic transmitter dipole moment as well as receiver noise threshold. The second topic revolves around determining the region of the earth surrounding the borehole that each different coil configuration is sensitive to, how that sensitivity varies spatially, and how changing the frequency of operation, the conductivity of the formation, and/or the source-receiver separation alters the sensitivity. Here we will focus on total field measurements due to the nature of the proposed tool. However, in many ways the analysis is equally valid for standard single sonde induction logging tools where the free space field is removed via bucking.

BACKGROUND

If we were to consider a more general case where 3D geologic structure is coupled with formation anisotropy, we would be able to define nine unique measurement configurations that employ magnetic field sources and sensors. However for simplicity, and to better understand the basic physics of the problem, we assume the background medium is a homogenous whole space of isotropic conductivity. Under these assumptions the nine sensor configurations reduce to the four unique configurations shown in Figure 2. It is easy to show that the remaining five configurations are either reciprocals and/or simple rotations of these four basic combinations.

In the following analysis we will make the simplifying assumptions that the transmitter consists of a magnetic dipole source and the magnetic field is a point measurement rather than an average over the length of receiver coil. Next we define a primary whole space field as the magnetic field at the receiver produced by a magnetic dipole source of moment $\mathbf{M}$ in a homogenous isotropic medium of conductivity σ.

Conductivity inhomogeneities that are embedded in this uniform material will give rise to scattered or secondary fields. Using the Born Approximation method in a manner similar to that of Moran (1982) and Spies and Habashy (1995), a set of equations are developed that relate the secondary or scattered magnetic fields measured by a receiver to a unit perturbation in conductivity at a certain point within the medium. These sensitivity functions, (or Frechet derivatives in the EM inversion problem), are used to estimate the resolution and sensing capability of different source-receiver-frequency combinations. In essence this method is the same as the *geometrical factor* approach of Gianzero and Anderson (1982) and Anderson (1986) for understanding induction log responses, with the main difference being only the manner in which the expressions are derived. The derivation of the Frechet derivatives under the assumptions outlined above is given in Appendix A.

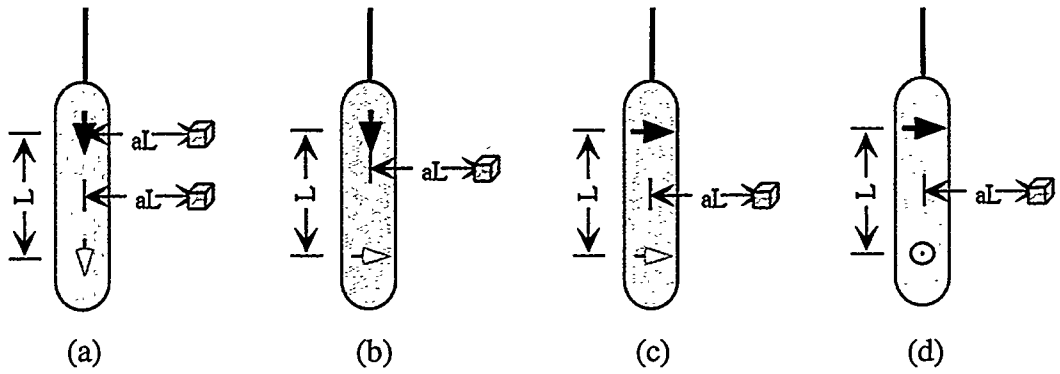

Figure 2 – The four unique source-receiver configurations for an induction logging tool located in a homogenous half-space. The arrows are defined in Figure 1. a) The coaxial configuration. b) The coaxial null-coupled configuration. c) Th coplanar configuration. d) The coplanar null coupled configuration.

Throughout this analysis, we wish to present the results in as versatile manner as possible such that they can be used for any source-receiver-frequency-formation conductivity configuration. Thus where ever possible the results are presented in terms of the 'induction number' defined as $l=\sigma\omega\mu L^2$. Here σ is the electrical conductivity of the isotropic medium, ω is the angular frequency of the source current (i.e. $2\pi f$ where f is the frequency in Hertz), μ is the magnetic permeability (assumed to be that of free space) and L

is the distance between the source and receiver (see Figure 2). The advantage to presenting the results in terms of the induction number is that if we normalize the sensitivity by the whole space primary field produced by the transmitter at the receiver, the resulting normalized value is identical for a constant induction number no matter what separation-frequency combination is employed, or what formation conductivity is encountered. Thus a single figure can provide valuable information for a wide variety of different scenarios.

In the following analysis, we study both the spatial variation in sensitivity as well as the signal to noise characteristics for the four different tool configurations shown in Figure 2 over a range of induction numbers. For the maximum coupled configurations (Figures 2a and 2c) we begin with a signal-to-noise analysis by studying how the total field within a homogenous whole space varies with induction number and source-receiver separation. Next, for all four configurations we study how the sensitivity changes with induction number for certain points in the medium surrounding the well, and at what induction numbers the scattered signal generated at a given point will be maximized. Finally we analyze the spatial variation of the sensitivity for all four configurations at a constant induction number using both 2D and 3D rendering formats.

COAXIAL (CA) CONFIGURATION

Although the standard commercially available logging induction logging tool has received much attention in the past in terms of defining its spatial sensitivity (e.g. Doll, 1949; Gianzero and Anderson, 1982; Moran, 1982; and Anderson, 1986), for completeness we include a full analysis of the coaxial configuration (Figure 2a). As outlined above, the first step of the analysis involves determining what combinations of source-receiver offset and frequency will yield high quality data. For this we assume two characteristics about our instrument; 1) the moment of the magnetic dipole transmitter is equal to 20 A-turns/m^2, and 2) the receiver noise threshold for the induction coil is 5 $\mu\gamma$, or approximately $4x10^{-9}$ A/m. These properties are rough averages derived from prototype tools that have been built, and for simplicity do not include variations that occur with changing frequency.

In Figure 3 we have plotted the magnetic field amplitude produced by the aforementioned magnetic dipole transmitter in a 0.1 S/m whole space. Each curve in this

plot represents a different source-receiver separation, and for reference we have also included the estimated sensor noise level. Notice that as the separation gets larger, the strength of the field at the receiver decreases, and thus the SNR decreases. Also notice that for a given source-receiver separation, the field is constant for induction numbers up to approximately 10. Above this point it decays rapidly with increasing induction number which is due to the attenuating effects of the conductive media, i.e., the skin effect.

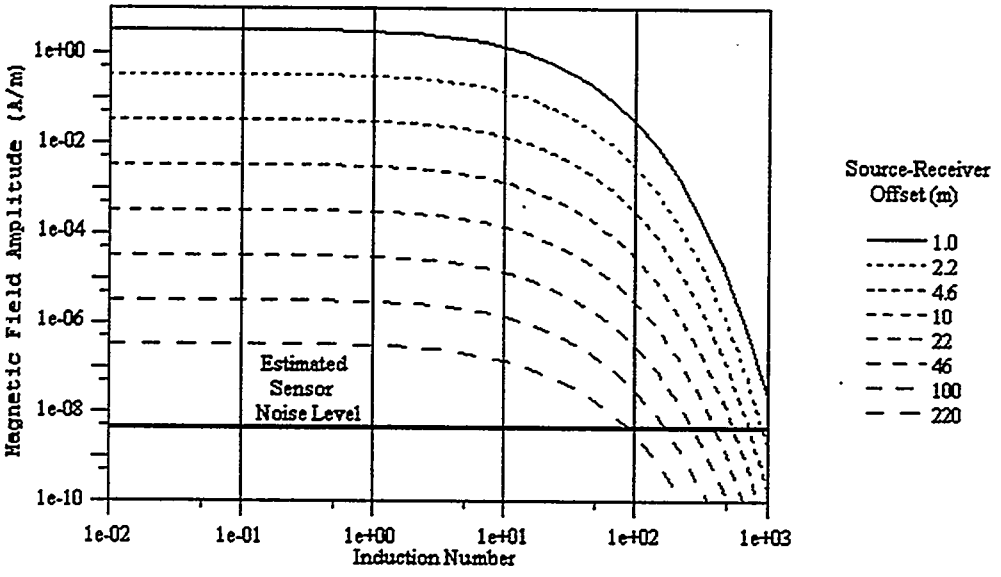

Figure 3 – The coaxial primary field as a function of induction number for different source-receiver separations. The magnetic dipole source has a moment of 20, and is located in a 0.1S/m whole space.

As demonstrated in Chapter IV, reasonable 3D image resolution can be achieved using total magnetic field data that exhibits a SNR of 100, that is the noise in the data is equal to 1% of the data amplitude. As figure 3 demonstrates, for induction numbers less than 1 there should be no problems collecting this quality.data except possibly for source-receiver separations greater than 100 m. As the induction number increases above 10, the field amplitude rapidly decreases such that for l=10, only separations less than 50m yield 1% data. If we increase l further to 1000 we find that none of the separations produce the desired results. Thus based on this initial analysis the tool should be built such that it

operates at induction numbers of 10 or less, and employs a maximum source-receiver separation of 100m or less.

In Figure 4 we have plotted the amplitude of the sensitivity given by Equation A-9 in Appendix A for seven different points in the medium, along with the primary field for a source-receiver separation of 10 m. The points lie on a line perpendicular to the center of the tool axis at different fractional distances of the source-receiver separation (aL) as shown in Figure2a. Each curve in Figure 4 represents the sensitivity versus induction number a different point. Notice that as aL increases, the induction number at which the sensitivity peaks decreases, i.e. for a given separation lower frequencies are required to maximize the scattering response as one moves away from the borehole. Also, as a is increased beyond 0.25, the maximum amplitude of the sensitivity decreases. This indicates that for regions progressively further away from the tool, a greater volume of scattering material is required to generate the same magnitude response as regions closer to the tool.

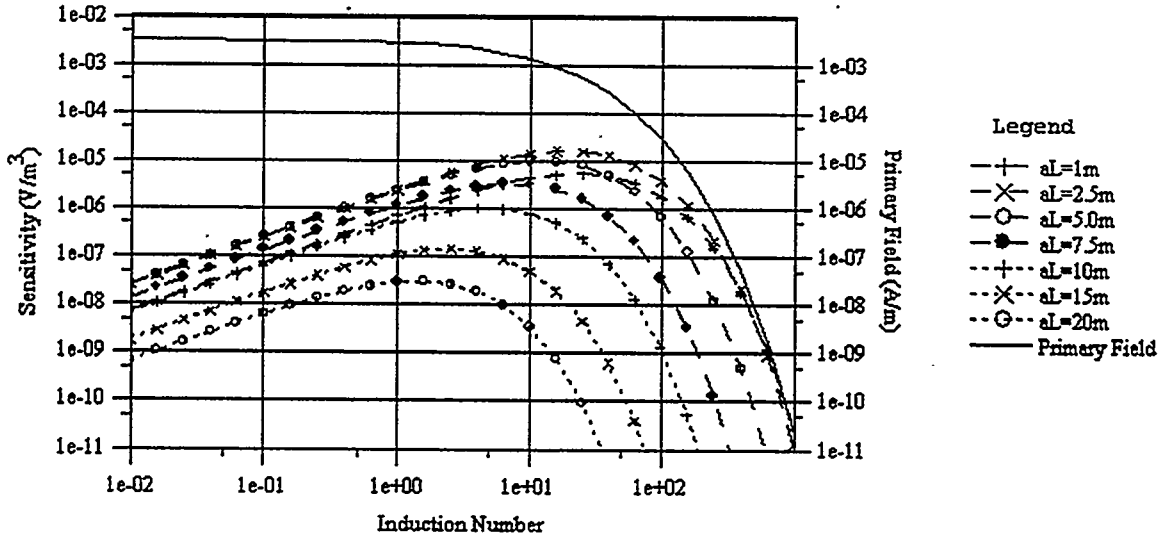

Figure 4 – The coaxial sensitivities and primary field as a function of induction number for a 10 m source-receiver offset. The seven different points where the sensitivity has been calculated are located along a line extending outward form the center of the tool as shown in Figure 2a. The transmitter is assumed to have a moment of 20 and is located within a 0.1S/m whole space.

The results in Figure 4 were produced using a source-receiver separation of 10m and a background conductivity of 0.1 S/m. To normalize the sensitivity plots such that they are fully dimensionless and don't depend on the source-receiver separation, the conductivity of the medium, or the frequency, we can divide the sensitivity curves by the primary field, and then multiply this result by the σL^3. Applying this normalization process to the curves shown in Figure 4 yields the results shown in Figure 5a.

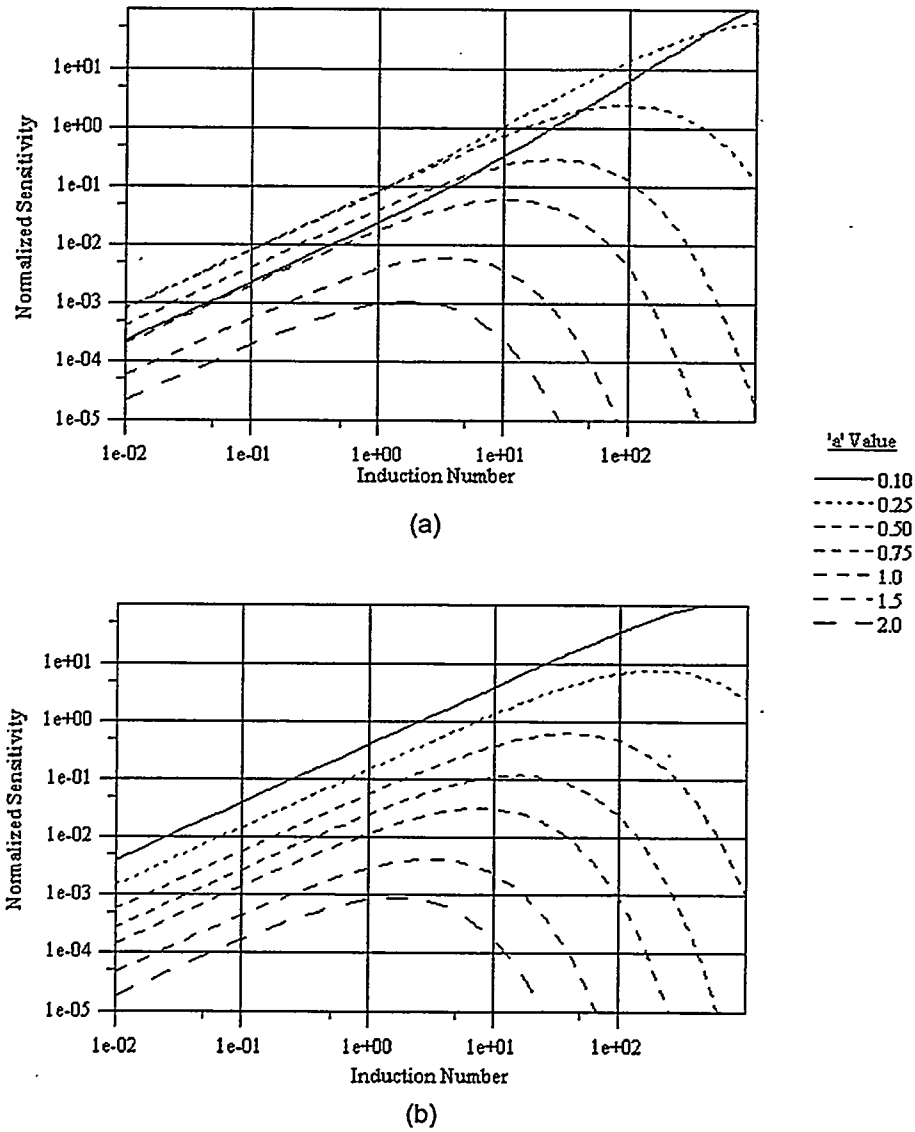

Figure 5 – Normalized coaxial sensitivities as a function of induction number for seven different points in the medium as shown in Figure 2a. a) The seven points are located radially away from the center of the tool. b) The seven points are located radially away from the transmitter end of the tool.

The primary function of this proposed tool is to detect and image 3D structure as far away from the well bore as feasibly possible. Thus the tool should operate in a range of induction numbers such that the sensitivity for those positions far from the well (here we define far to be 1.5L to 2L) is as large as possible with relation to sensitivities closer in. It would appear from Figure 5a that the low end for a total field measurement is around an induction number of 0.1. This ensures that the sensitivities further from the well are not substantially smaller than those for positions closer to the well, yet are also not substantially less than the primary field. The latter is required for signal to noise considerations. If we combine this result with the upper bound on induction numbers of 10 that was determined from Figure 3, we have effectively constrained the range of operation of a total field logging tool to lie between induction numbers of 0.1 and 10. Notice that in this range the normalized sensitivity amplitude peaks for distances L to 2L away from the well bore. Also, for a distance L away from the borehole the sensitivity is within 1 order of magnitude of the maximum sensitivity closer to the borehole, while for a distance of 2L away from the tool, the sensitivity is within 2 to 4 orders of magnitude of those maximum sensitivities.

An additional interesting point to note is the behavior of the sensitivity curves for induction numbers less than 0.1. As the induction number is decreased beyond this point, the sensitivity amplitude for each point decreases. However, note that the rate of decrease with induction number is constant, and the curves parallel each other. This implies that the ratio between the near well bore sensitivity, and the sensitivity at L to 2L away from the borehole will remain constant with decreasing induction number. Thus for a fixed source-receiver separation and formation conductivity, simply decreasing the frequency below a certain point will not yield deeper 'penetration' as the sensitivity near the well bore will continue to dominate the response.

In Figure 5b we have plotted the normalized sensitivities for the same distances away from the well bore as were analyzed in Figure 5a, except in this case the analysis is confined to the transmitter depth rather than the mid-point of the tool (Figure 2a). It must be noted that due to reciprocity of this configuration when located within a whole space, this set of results is identical to those located near the receiver. Although there are differences between the two sets of sensitivity curves (Figure 5a and Figure 5b), in general they are very similar.

The most notable difference occurs for a=0.1. The greater sensitivity in Figure 5b for this point closest to the well bore indicates that the sensitivity is largest near the transmitter (and receiver), and that it decreases away. Also notice that for "a" values of 0.25 to 1.0, the sensitivity magnitudes along the line adjacent to the transmitter are less than those near the center of the tool, and that for separations of 1.5 and 2.0 the sensitivities are approximately the same. A more thorough analysis of the spatial variability of the sensitivity is given below.

Figure 5 is a very useful tool for designing a total field - long offset logging system. For example, let us assume that we wish to characterize the media surrounding a borehole to a distance of 10m away from the well. If the tool is operating at an induction number of 10 and the source-receiver separation is 10m, Figure 5a indicates that the sensitivity for the region of interest is approximately 1.5 orders of magnitude less than the maximum sensitivity that occurs for a point at 2.5m away from the well. Employing the same separation but decreasing the frequency such that the system is operating at an induction number of 1 yields sensitivities within the target zone that are now less than one order of magnitude less than the near well bore sensitivity. Thus this configuration should better delineate formation variations within the region of interest from those occurring near the borehole. However, because the noise level of the receiver is constant, and because decreasing the induction number effectively decreases the magnitude of the tool sensitivity to the region of interest, we have effectively decreased our SNR by a factor of 5.

Next we investigate reducing the source-receiver separation, i.e. the tool length, to 5m in order to make down hole deployment more manageable. To investigate a region 10m away from the well now requires the analysis of the difference between the a=2.0 and a=0.25 curves. At an induction number of 10 the 2.0L sensitivity is over 3.5 orders of magnitude less than the maximum sensitivity, while at an induction number of 1 it is approximately 2 orders less. Thus it would be more difficult to distinguish inhomogeneity within the region of interest to that near the borehole with this source-receiver configuration. The difference between the maximum and minimum sensitivities can be decreased somewhat by lowering the frequency to correspond to an induction number 0.1 as long as the signal to noise ratio is still favorable. However, this still will not provide as small a ratio between the sensitivities generated near to and far from the borehole as if larger

separations are employed. Combining this with the analysis given in the last paragraph indicates that in order to maximize the measurable response of regions far away from the well, the tool should employ as large a source-receiver separation as feasibly possible given the nature of the down hole environment. In addition, the frequency that is employed should be as low as the signal to noise characteristics of the system will allow.

To better analyze how the response of the formation to the tool varies spatially, we have plotted the sensitivity as a function of spatial position in 2d (Figure 6) and 3d (Figure 7) for a single induction number of 1.0. The values displayed in these figures have been processed in the same manner suggested by Spies and Habashy (1995), where the real and quadrature sensitivities are calculated at a constant interval across a grid and plotted on a logarithmic scale with red representing positive sensitivity and blue negative values. The maximum on the grid is assigned a value of 60dB's, and all other values scaled accordingly, with amplitudes less than 1dB set to zero. Thus in Figure 6 and all other subsequent 2D plots we are showing those values which are within three orders of magnitude of the maximum sensitivity.

In the 3D renderings, for example Figure 7, the $\pm$ 20dB isosurface has been plotted. Thus the 3D volume (or volumes) encloses sensitivities that are down to two orders of magnitude less than maximum value. Note that all spatial axes in these plots have been normalized by the coil separation such that the plots are again dimensionless.

Comparing Figure 6 to figures published in earlier papers indicates that these plots closely resemble the geometrical factor plots originally introduced by Doll (1949; Figure 6) for simple two-coil induction tool analysis, and later modified by Anderson (1986; Figures 39 and 40) for the analysis of more sophisticated medium and deep induction logging tools. In those cases the medium was assumed to exhibit a cylindrically symmetric geometry about the borehole, while here we assume full three dimensionality. There is a second major difference between the earlier results of Doll (1949) and those presented here in that the conductivity of the medium is not taken into account in Doll's geometrical factor calculations. Thus the attenuating effects of the formation on the signal are not apparent.

Here, as in the work of Moran (1982), these effects are accounted for, and thus a more accurate interpretation of the spatial variation of the sensitivity about the tool is achieved.

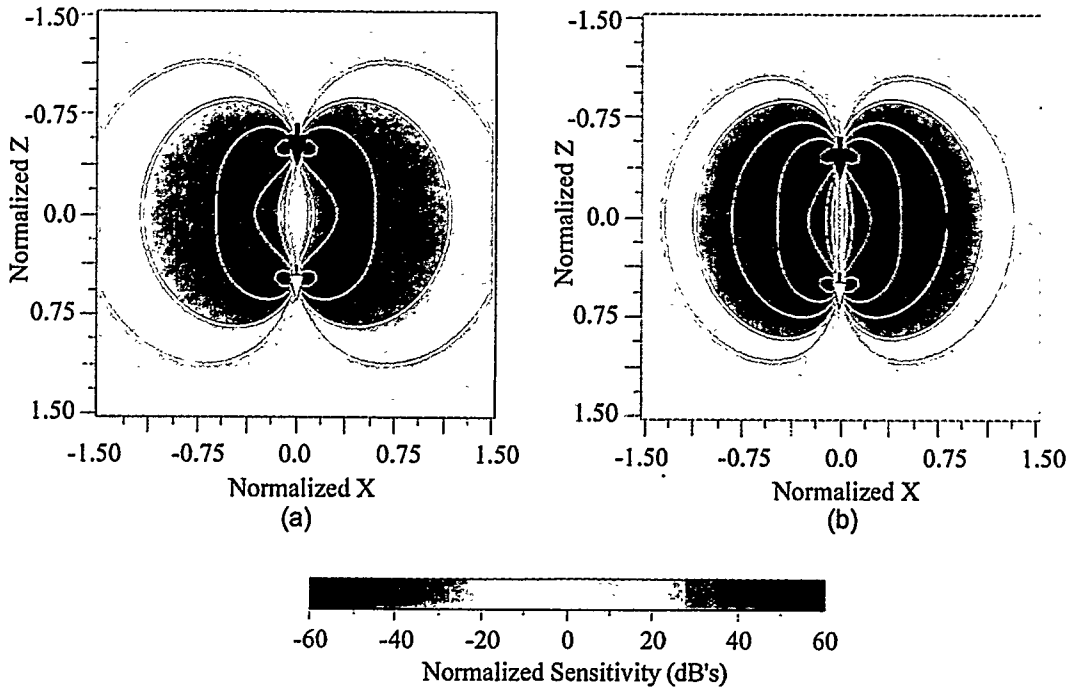

Figure 6 – Logarithmically normalized coaxial sensitivity as a function of position in the y=0 plane for an induction number of 1. The results have been normalized as described in the text. a) Real (resistive) component. b) Quadrature (reactive) component.

A quick analysis of Figures 6 and 7 show that as indicated by comparing Figure 5b to Figure 5a, the sensitivity peaks near the source and receiver. Also note that like the geometrical plots of Doll (1949), the sensitivity is symmetric about the borehole even though we are assuming a 3D rather than 2D cylindrical geometry. This symmetry is due to the fact that we have assumed a homogenous whole space for these calculations. If we were to apply this approach to a more general 3D model, then the resulting sensitivity plots would exhibit an asymmetric nature. However, also note that due to the cylindrical symmetry we can not delineate a scattering target on one side of the borehole from one on the opposite side. Rather, all that can be determined is the location of the target along the borehole, and if multiple frequency measurements are made, the radial position away from the borehole of the body.

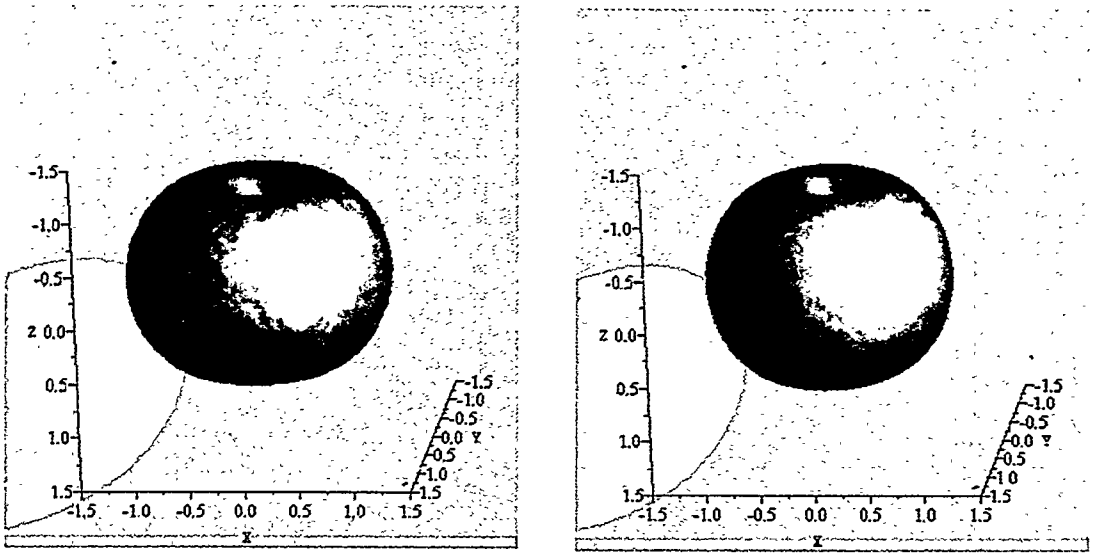

(a) (b)

Figure 7 – Three dimensional isosurface corresponding to the –20dB level of the logarithmically normalized coaxial sensitivity. The sensitivity has been normalized as described in the text. a) Real (resistive) component. b) Quadrature (reactive) component.

This analysis has focussed on the standard coaxial tool configuration which has been analyzed extensively in the past. Thus to this point nothing new has been presented regarding induction logging. However in the next three sections we will analyze the sensitivity for non-traditional induction tool configurations, and demonstrate how 3D information can be ascertained as long as the proper measurements are made.

COAXIAL NULL-COUPLED (CANC) CONFIGURATION

In Figure 8 we have plotted the normalized sensitivities at 7 points away from the tool for the coaxial null-coupled (CANC) coil configuration shown in Figure 2b. Note that this configuration employs the same source polarization as the coaxial, but the receiver is rotated 90 degrees such that it measures the x (or y) component of the magnetic field. Because there is no primary or whole space magnetic field for this configuration, the results have been normalized by the same coaxial primary field as employed for the CA system in Figure 5. Thus these curves can be compared directly to the curves for the coaxial configuration shown in Figure 5a. However there is one major difference between this set

of curves and those in Figure 5a in that the points of interest are located along a horizontal line that extends outward 0.25L below the transmitter rather than half way between the source and receiver. The reason for this will be become apparent in the 2D and 3D analyses that follow.

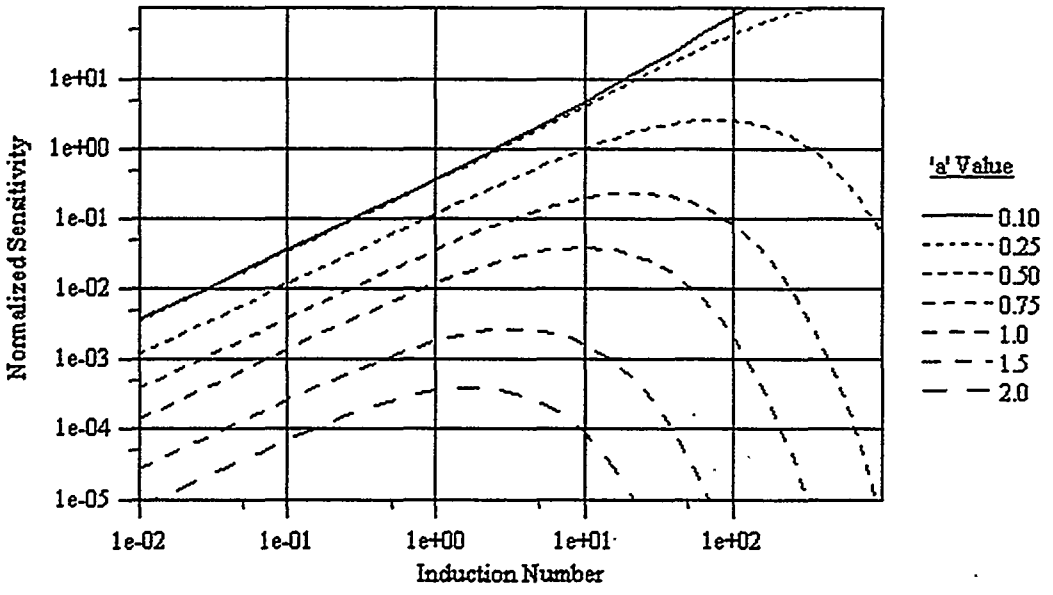

Figure 8 – Normalized coaxial null coupled sensitivities as a function of induction number for seven different points in the medium. The seven points are located radially away from the center of the tool at a distance 0.25L below the transmitter as shown in Figure 2b.

Comparing Figure 8 to Figure 5a shows that the sensitivities CA and CANC configurations behave in a similar manner with respect to induction number, both in shape and amplitude. The fact that the amplitudes are similar ensures that the signals generated by this configuration are measurable given the SNR characteristics of the system. However, for the CANC configuration, the magnitude of the sensitivity near the borehole ($a \leq 0.5$) is larger than those for the CA mode, and smaller for those points further away from the well. This indicates that this configuration is not as efficient for sensing regions greater than 0.5L away from the borehole when compared to a standard coaxial tool. In addition the sensors employed to measure the horizontal fields are noisier than a vertical sensor (see the section on the coplanar configuration below). Thus if the signal to noise characteristics of the

receiver are taken into account, these curves are even smaller in magnitude when compared to those in Figure 5.

With these drawbacks compared to the CA arrangement, it might be difficult to understand why the CANC configuration is important. However the utility of this coil arrangement for delineating 3D structures becomes apparent when the 2D (Figure 9) and 3D renderings (Figure 10) are analyzed. Notice that both the real and quadrature sensitivity change sign but are equal in amplitude on opposite sides of the borehole. This indicates that the scattered fields generated by inhomogeneities located the same distance away from the tool, but in different directions, will be of the same amplitude but differ in phase by 180°. Also note from Figure 10 that there is no sensitivity to regions located along the x=0 plane. The response to these regions is provided by measuring the y component of the magnetic field in conjunction with the x component. Thus the sensitivities generated by this configuration are identical to those shown in Figures 9 and 10 but rotated by 90° around the z axis. A tool configuration consisting of a transmitter whose moment is aligned parallel to the borehole, and two receivers aligned perpendicular to the borehole as well as to each other will produce magnetic field amplitude, and more importantly phase data from which 3D structure can be ascertained. In fact, this dual CANC configuration is the only tool configuration of the four shown in Figure 2 that provides true 3D information of the region surrounding the borehole, and thus it is essential for the success of a 3D tool. This will become evident as we examine the two remaining configurations (Figure 2c and 2d).

On a final note, there has not been an explanation why Figure 8 employed points that were not located along a line projected outward from the center of the tool. The reason for this becomes obvious from Figures 9 and 10 which show the maximum 'extension' of the sensitivity away from the tool occurs at a distance of approximately 0.25L away from the source toward the receiver. Also a comparison of Figures 9 and 10 with Figures 6 and 7 show that this configuration is not as sensitive to regions 1.0 to 2.0L away from the borehole as the standard CA tool which verifies the sensitivity analysis derived from Figure 8.

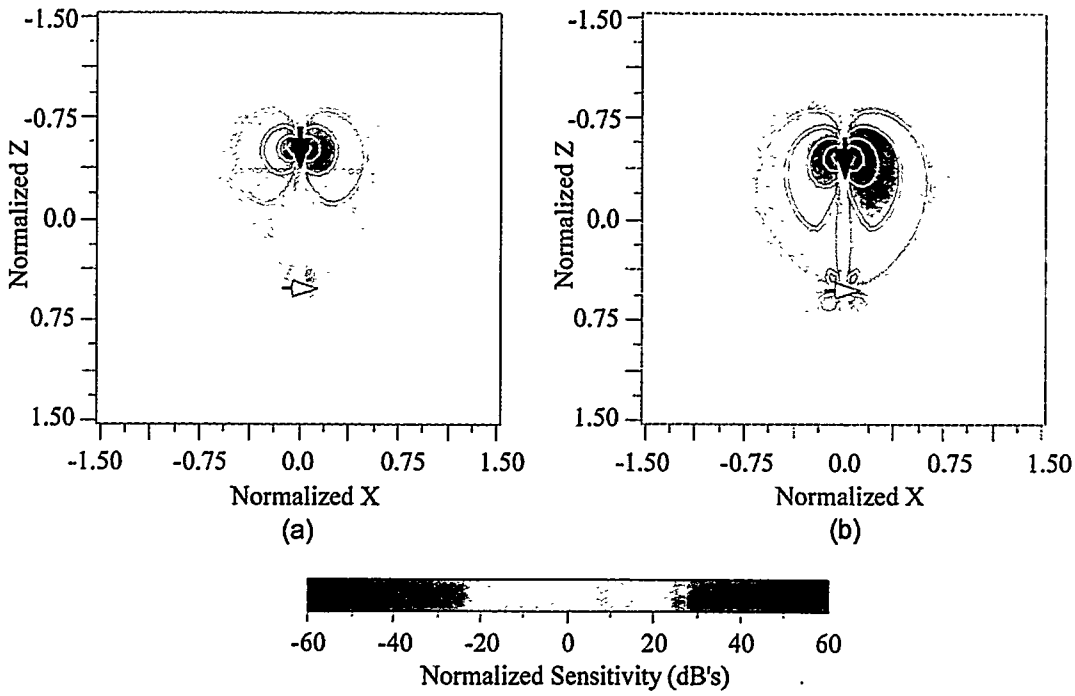

Figure 9 – Logarithmically normalized coaxial null coupled sensitivity as a function of position in the y=0 plane for an induction number of 1. The results have been normalized as described in the text. a) Real (resistive) component. b) Quadrature (reactive) component.

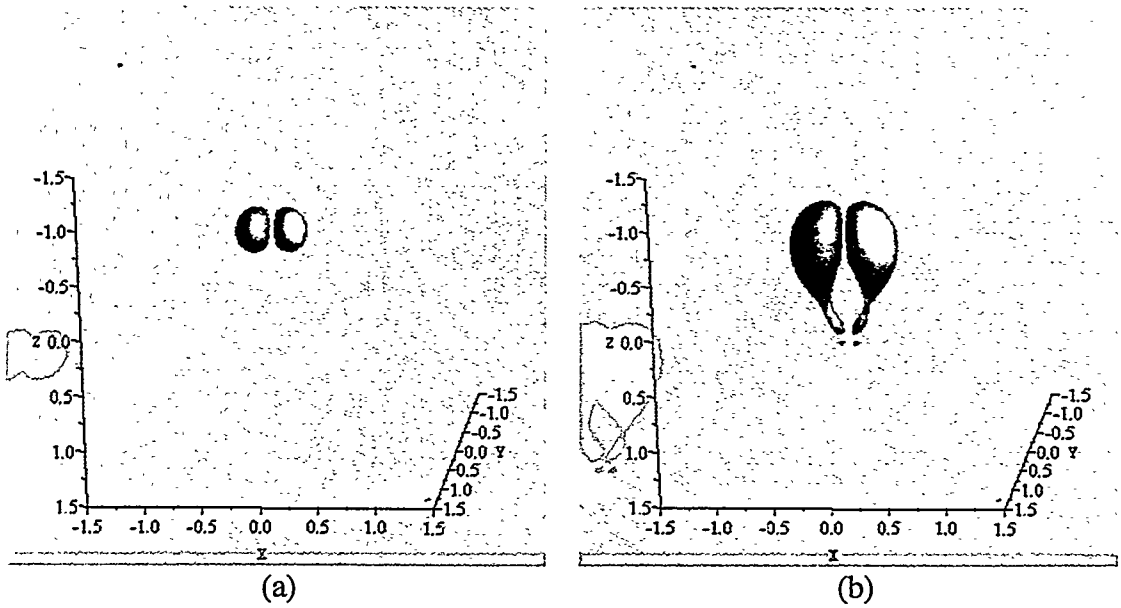

Figure 10 – Three dimensional isosurface corresponding to the –20dB level of the logarithmically normalized coaxial null coupled sensitivity. The sensitivity has been normalized as described in the text. a) Real (resistive) component. b) Quadrature (reactive) component.

COPLANAR (CP) CONFIGURATION

The coplanar configuration shown in Figure 2c is commonly used for surface prospecting, but rarely in a borehole logging configuration for reasons that will become apparent. In Figure 11 we have plotted the whole space primary field generated by the CP arrangement. Here we have assumed a magnetic dipole transmitter moment of 5 A-turns/m^2, and a receiver noise threshold of 20 $\mu\gamma$, or approximately 1.6x10-8 A/m.

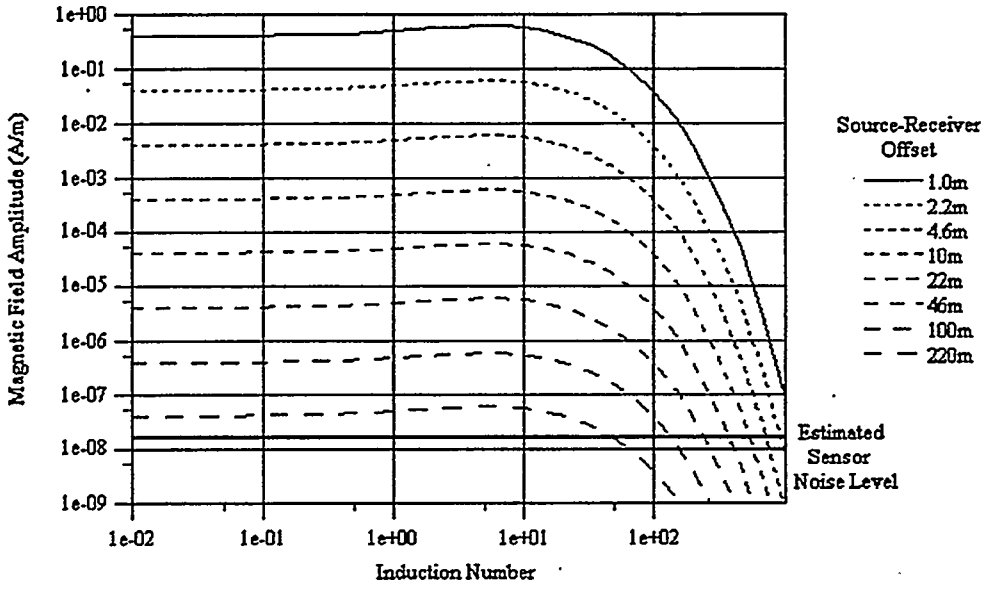

Figure 11 – The coplanar primary field as a function of induction number for different source-receiver separations. The magnetic dipole source has a moment of 5, and is located in a 0.1S/m whole space.

Notice that the system signal-to-noise characteristics are worse for this configuration when compared to the same calculations for the CA arrangement given in Figure 3. There are two primary reasons for this. First, the primary field magnitude for this configuration is ½ the value of the CA configuration for the same source-receiver separation. Second, the transmitters and receivers are more difficult to build to the same accuracy specifications as the CA system. The latter results from the fact that for the vertically oriented transmitter and receiver coils used in the CA system, the windings are horizontal about then axis of the tool. This configuration is optimal for placing the coils in a long, narrow tube that can be lowered down a borehole, and for making use of high permeability cores that boost the magnetic field. For the horizontal coils employed in the CP configuration, we must either use several

smaller coils in parallel, or a coil that is long in one direction but very narrow. Thus the sensors are not optimized with regards to either use of space or the incorporation of core materials which results in a lower moment for the source, and a higher noise floor in the receiver. Analyzing Figure 11 more closely indicates that the maximum source-receiver separation at which we can operate while producing measurements that are good to 1% is approximately 70m. Thus if we wish to build a tool containing all four coil configurations and using the same source-receiver offset for all configurations, the maximum separation between the source and receiver will be limited by the SNR characteristics of this particular configuration.

In Figure 12 we have plotted the normalized sensitivities for different points located radially outward from the center of the tool in the x-(Figure 12a) and the y- directions (Figure 12b). Notice that comparing these results to those in Figure 5a, the CP configuration is more sensitive to the near borehole region than the CA tool. This coupled with the fact that the normalized sensitivities at a distance of L or greater from the well are equal in magnitude to, or less than, those for the CA arrangement indicates that the CP configuration is going to produce less of a response to regions outside of the immediate vicinity of the borehole. The problem is further accentuated by the poorer signal to noise characteristics of the CP system.

Although the CP arrangement might not have the depth sensitivity of the CA system, it does offer some benefits over the latter in terms of directional sensitivity. This becomes evident when Figures 12a and 12b are compared to each other, and when we analyze the 2D cross sections through the volume in the x (Figure 13) and y (Figure 14) directions. Notice that near the borehole the two plots exhibit approximately the same sensitivity pattern. However at a distance of 0.5L away from the borehole, the sensitivity in the Y direction goes to zero, and for distances that are greater than this, the sensitivity as a function of position in the two directions behaves differently. This contrasts to the CA arrangement which demonstrates a cylindrical symmetry about the borehole (see Figure 7), i.e. no directional sensitivity. However, also notice that the directional sensitivity obtained with the CP configuration is not a true 3D sensitivity like that produced with the CANC

configuration. That is, inhomogeneieties on opposite sides of the borehole are indistinguishable from one another in terms of position.

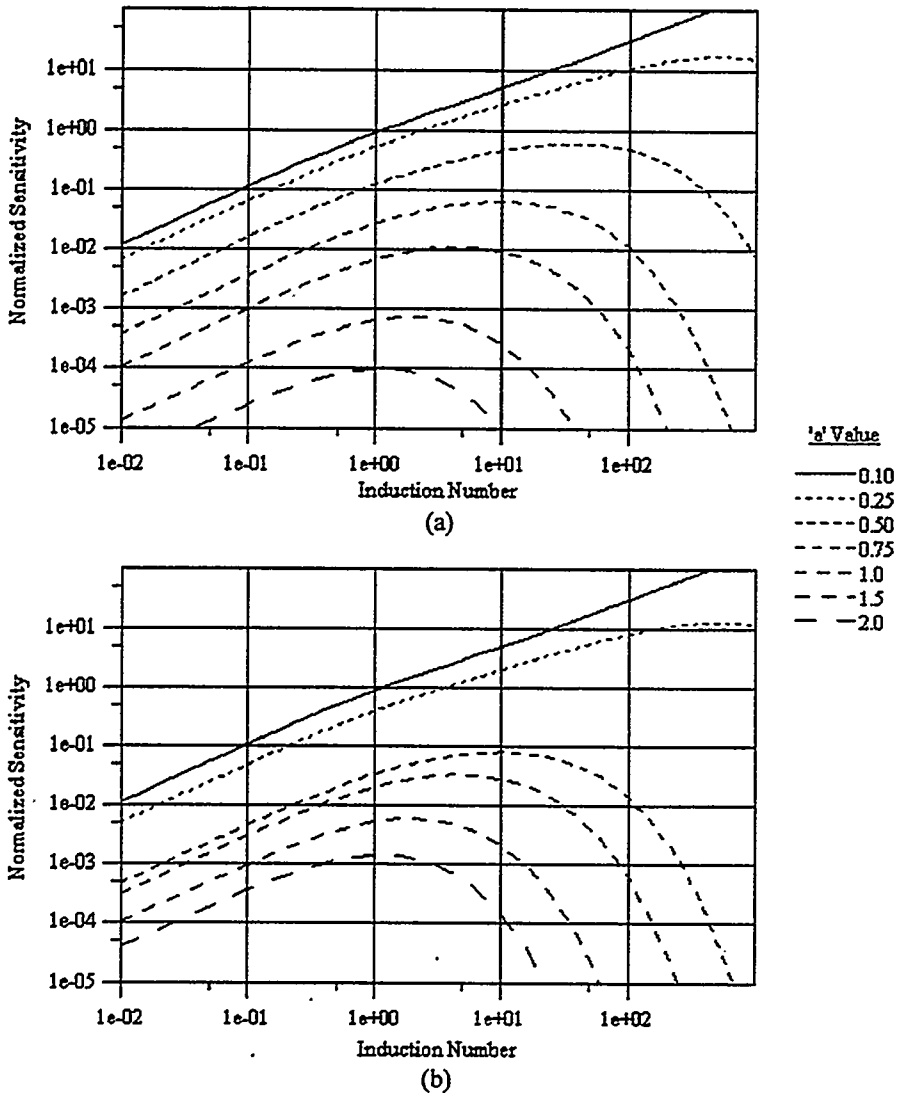

Figure 12 – Normalized coplanar sensitivities as a function of induction number for seven different points in the medium. a) The seven points are located radially away from the center of the tool in the x direction as shown in Figure 2c. b) The seven points are located radially away from the center of the tool in the y direction.

In figure 15 the ±20dB isosurface is plotted in three dimensions. Again the limited sensitivity with distance away from the well becomes apparent by comparing this figure to the 3D volume representation for the CA configuration (Figure 7). Another interesting note is the rapid phase shift that occurs on opposite sides of the transmitter and receiver. This

phenomenon is apparent in the 2D plots given in Figures 13 and 14, but is much more striking in 3D. This characteristic should provide for excellent resolution in the direction along the borehole, although the change in sign may make interpretation of the raw data difficult.

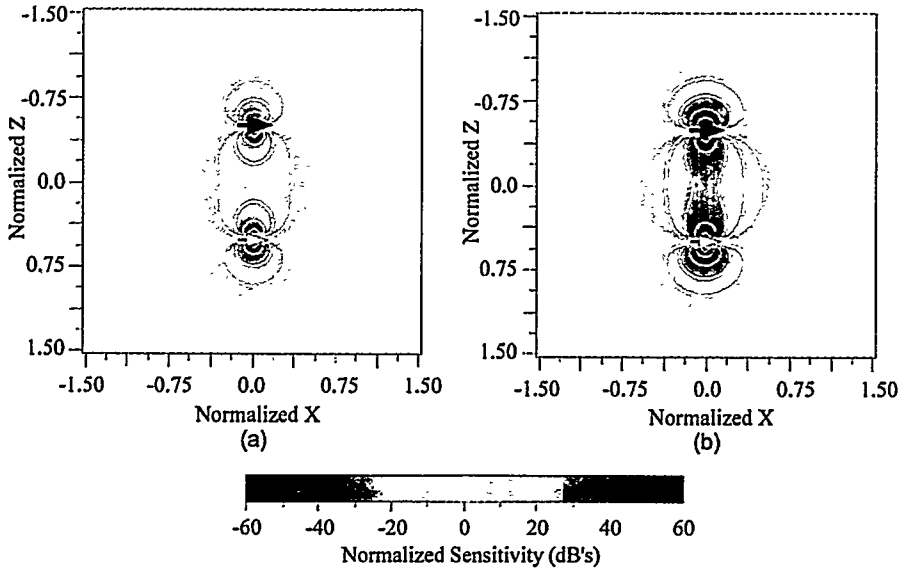

Figure 13 – Logarithmically normalized coplanar sensitivity as a function of position in the y=0 plane for an induction number of 1. The results have been normalized as described in the text. a) Real (resistive) component. b) Quadrature (reactive) component.

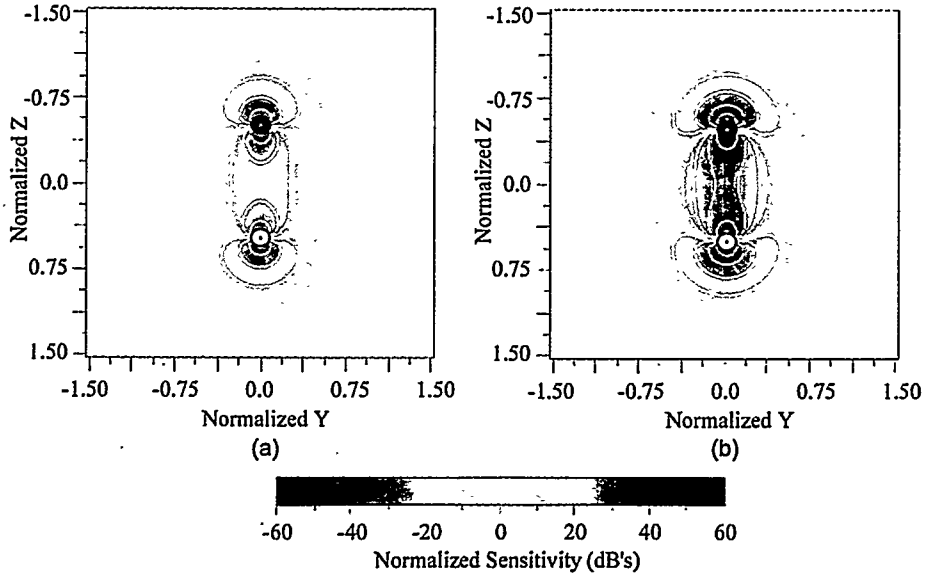

Figure 14 – Logarithmically normalized coplanar sensitivity as a function of position in the x=0 plane for an induction number of 1. The results have been normalized as described in the text. a) Real (resistive) component. b) Quadrature (reactive) component.

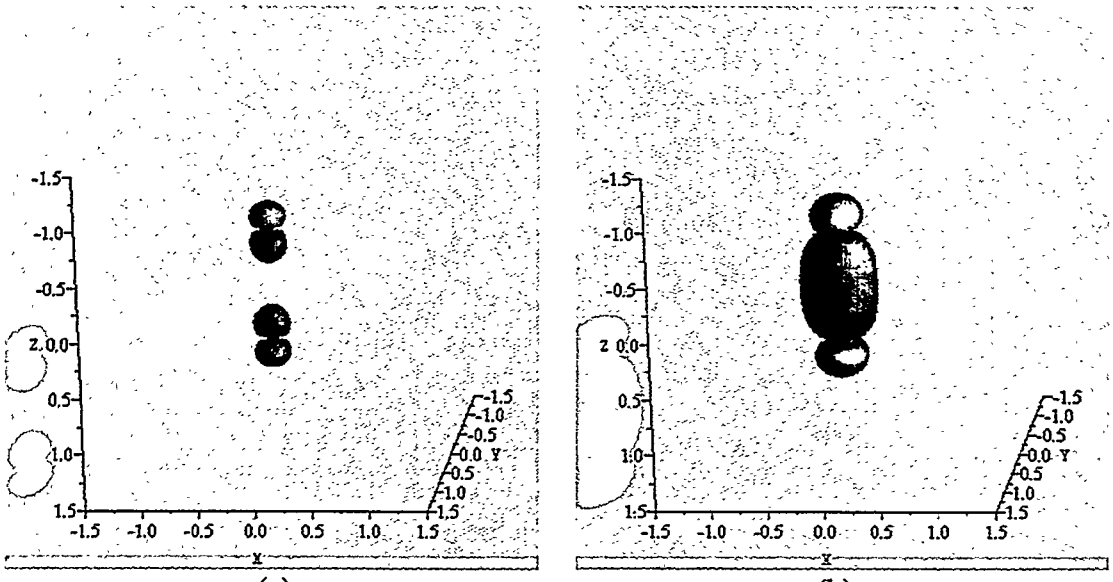

(a) (b)

Figure 15 – Three dimensional isosurface corresponding to the –20dB level of the logarithmically normalized coplanar sensitivity. The sensitivity has been normalized as described in the text. a) Real (resistive) component. b) Quadrature (reactive) component.

COPLANAR NULL-COUPLED (CPNC) CONFIGURATION

The last unique configuration to study is the CPNC arrangement shown in Figure 2D. In this case the axis of the source and receiver are both perpendicular to the borehole, but unlike the CP configuration they are also perpendicular to each other. Thus a 90° 'twist' around the axis of the coplanar tool has been applied to produce the CPNC arrangement.

The normalized sensitivities versus induction number for different locations away from the tool have been plotted in Figure 16. Because there is no whole space primary field for this arrangement, that of the CP configuration has been employed in the normalization process. Also note that the sensitivity has been calculated at points along the x=y diagonal rather than the x axis. The reason for this will become apparent in a moment.

Notice that compared to Figure 12, Figure 16 shows that the sensitivity of the CPNC arrangement to the region immediately surrounding the well bore is less than that of the CP configuration. Thus a tool built with this configuration should provide for better resolution with increasing distance away from the well bore. Also, notice by comparing Figure 16 to Figure 5a that the sensitivity magnitudes for the CPNC arrangement show the same characteristics as the CA arrangement, but on average are approximately 1 order of

magnitude less than for the CA tool. Thus the two tools will have similar resolution with depth away from the borehole, although the CA tool will yield data with better SNR characteristics. This general similarity of depth sensitivity between the tool configurations becomes even more apparent when we compare the 2D cross sections along the x=y diagonal for the CPNC system (Figure 17) to that of the CA configuration along the x axis (Figure 6).

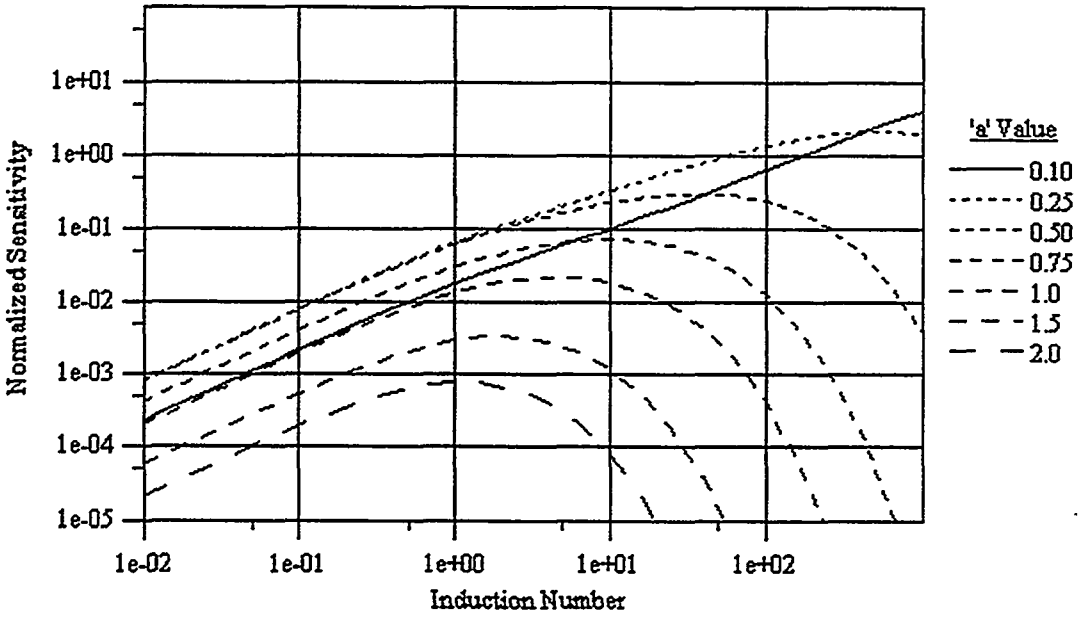

Figure 16 – Normalized coplanar null coupled sensitivities as a function of induction number for seven different points in the medium. The seven points are located radially away from the center of the tool along the x=y diagonal.

There is, however, a major difference between the resolving capability of the CPNC system and the other configurations that becomes apparent only when the 3D volumetric representation of the sensitivity is presented (Figure 18). Note that alternating 'lobes' of positive and negative sensitivity are located in the four quadrants of the xy plane, and that the sensitivity is zero along the x and y axes. The latter observation illustrates the reason for plotting the point and 2D sensitivities along the x=y diagonal. Because the sensitivity shows alternating signs across the different axes, this configuration will offer excellent

directional sensitivity, and when combined with the other configurations, increased resolution will be the result. Once again, however, like the CP configuration the CPNC arrangement does not offer true 3D information as a target located on one side of the well will produce the same response as if it were located 180° on the other side of the borehole.

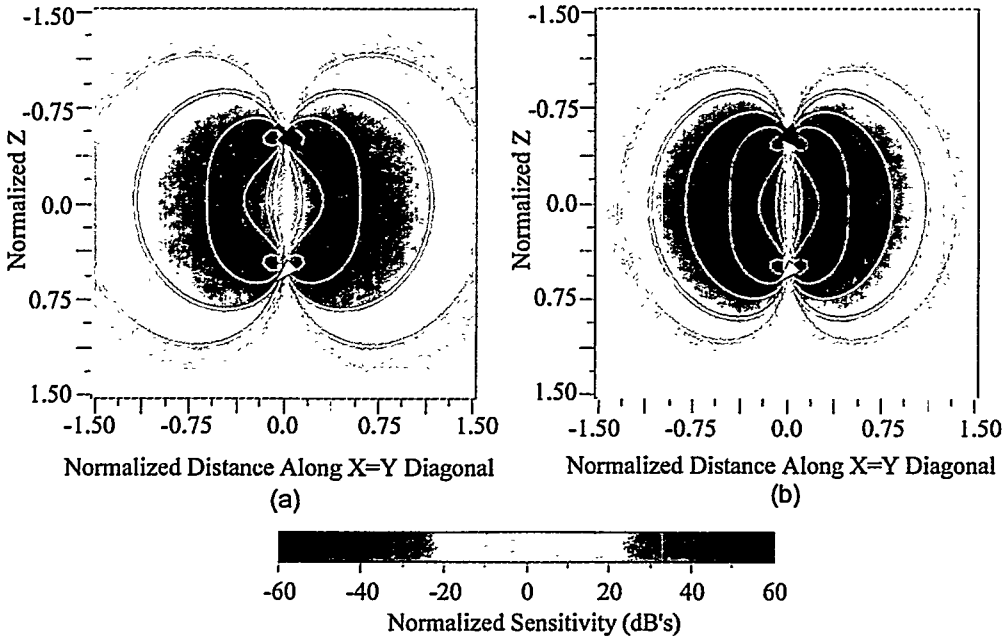

Figure 17 – Logarithmically normalized coplanar null coupled sensitivity as a function of position in the x=y plane for an induction number of 1. The results have been normalized as described in the text. a) Real (resistive) component. b) Quadrature (reactive) component.

This sensitivity analysis has been conducted assuming a homogenous earth model. In addition we have made very simplifying assumptions about the character of the noise that would be present in the measurements. In fact we have not even addressed the presence of mispositioning noise that could be present due to 1) rotation between the different transmitter and receivers, and 2) deviations in wells causing transmitters and receivers to no longer be properly alligned. In the next chapter we present a simple numerical modeling study to validate the sensitivity study presented here and to investigate the problems associated with mispositioning of the various tools associated with a multi-sonde configuration.

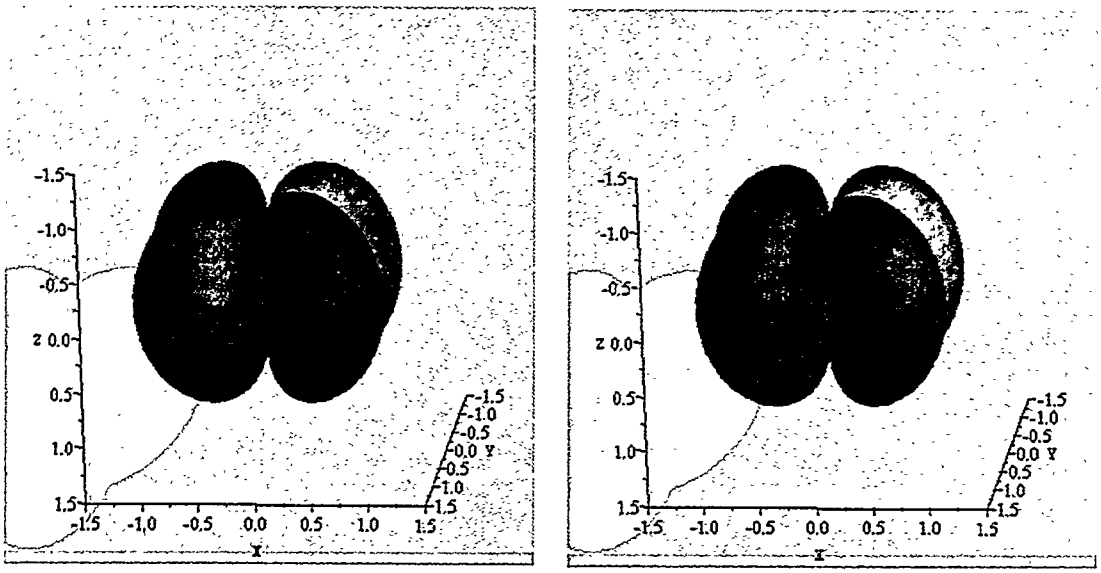

(a) (b)

Figure 18 – Three dimensional isosurface corresponding to the –20dB level of the logarithmically normalized coplanar null coupled sensitivity. The sensitivity has been normalized as described in the text. a) Real (resistive) component. b) Quadrature (reactive) component.

CHAPTER III

FORWARD MODELING STUDY

In order to numerically demonstrate that 3D information is available from three component induction logging measurements, and to verify conclusions made within the previous chapter, we will employ the 3D finite difference forward modeling scheme presented in Alumbaugh et al. (1996). The models employed in this analysis consist of two different tabular bodies located off axis from the borehole as shown in Figure 19. The difference between the two models is that the body in Figure 19a has been rotated around the z axis by 180° to produce the model in Figure 19b. Thus the shape of the two bodies is identical and the only difference in the tool response will be due to the difference in positioning. Also notice that the borehole has not been included in these models as it has been assumed for the source-receiver offsets employed here the borehole effect is negligible (this will be discussed later).

In the following analysis results have been computed at 10 KHz and 100 KHz. At 10 KHz a source-receiver separation of 16m is employed, while at 100 KHz a separation of 6m is used. Because the whole space conductivity (σ) is 0.1S/m, the two different scenarios correspond to induction numbers, $l=\sigma\omega\mu L^2$, of 2.7 and 2.1, respectively. Here ω is the angular frequency (i.e. $2\pi f$ where f is the frequency in Hertz), μ is the magnetic permeability (assumed to be that of free space) and L is the distance between the source and receiver.

SOURCE ALIGNED PARALLEL TO THE BOREHOLE AXIS

In Figure 20 we have plotted the magnetic field amplitude and phase for both frequencies and models that result when a vertical magnetic dipole (VMD) source aligned with the axis of the borehole is employed to excite the medium. Notice from Figure 20a that for the coaxial (CA) configuration where the vertical magnetic field is measured that the perturbation generated by the target is 6% in amplitude and 5° in phase at 10KHz, and 10% in amplitude 3° in phase at 100KHz. Also from Figure 20b we see that the maximum amplitude of the x directed coaxial null coupled (CANC) fields produced by the target is approximately 10% of the primary field. Because the estimated signal to noise

characteristics of the measurement system is 1% in amplitude and 0.5° in phase, we believe that the response of the target zone can easily be measured for both the direct and null coupled components of the field.

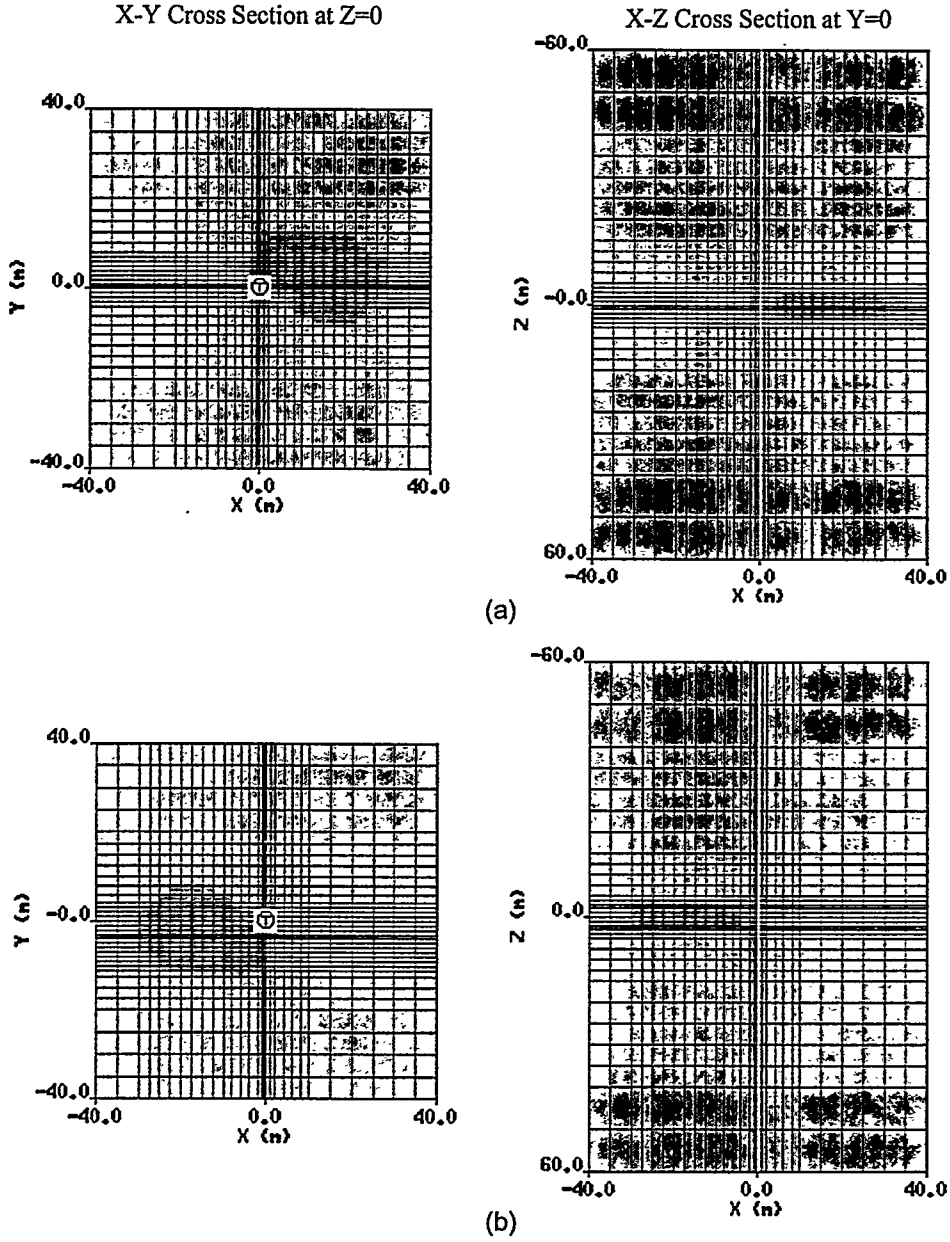

Figure 19 – Models used in the forward modeling analysis of different coil configurations. Model 2 in Figure (b) is identical to Model 1 shown in Figure (a) except it has been rotated around the z axis by 180°. The 3D body represented by the red region is 8m thick and has a conductivity of 0.5S/m. The background (blue) has a conductivity of 0.1S/m.

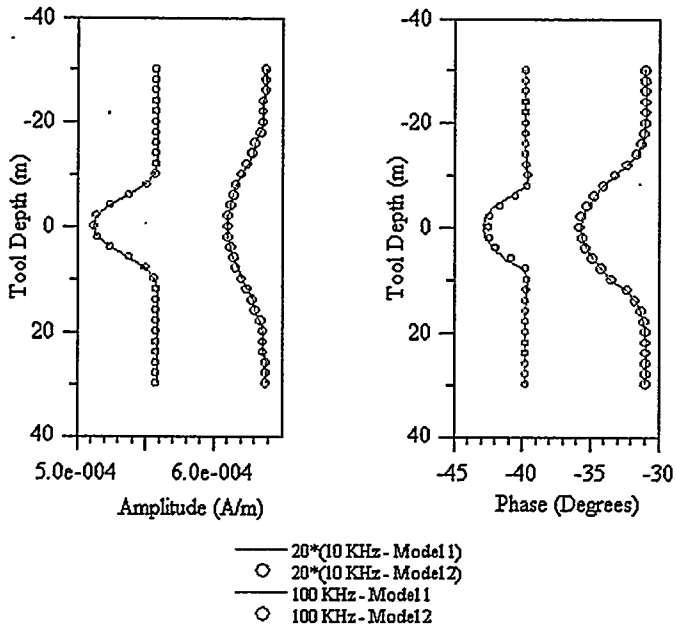

(a)

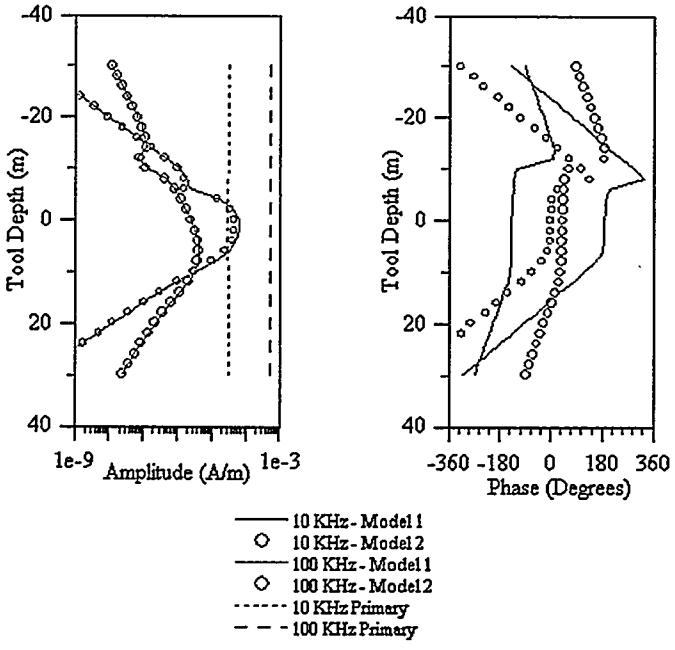

(b)

Figure 20 – Forward simulations of models shown in Figure 19 for a source aligned parallel to the axis of the borehole. a) Results for coaxial configuration where the field parallel to the borehole is measured. Note that the amplitude at 10Khz has been multiplied by 20 to fit on the same scale as the 100 KHz results. b) Results for the coaxial null coupled configuration where the field in the x direction perpendicular to the borehole axis is measured.

Notice that the vertical field amplitude and phase in Figure 20a is identical for the two models, and thus there is no 3D information present in CA measurement. However, although the amplitude response of the CANC configuration in Figure 20b is identical for the two models, the phase response differs by 180 degrees. As also indicated by the sensitivity study in the last chapter it is this horizontal field phase information that is the critical component required in order to reconstruct the 3D structure of the medium.

To demonstrate that the two orthogonal components of the CANC configuration differ in terms of their directional sensitivity, in Figure 21 we have plotted the Hx and Hy fields at 10 KHz for the model in Figure 19a. Notice that although the phase of the two components is nearly identical, the amplitude of the Hx field is almost twice as large as that of the Hy field. Using Figures 9 and 10 along with Figure 19a we realize that this difference in amplitude is due to a greater amount of anomalous conductivity being located about the x=0 plane than is located about the y=0 plane. Because of this larger amount of conductive material in the x direction, the Hx field is larger.

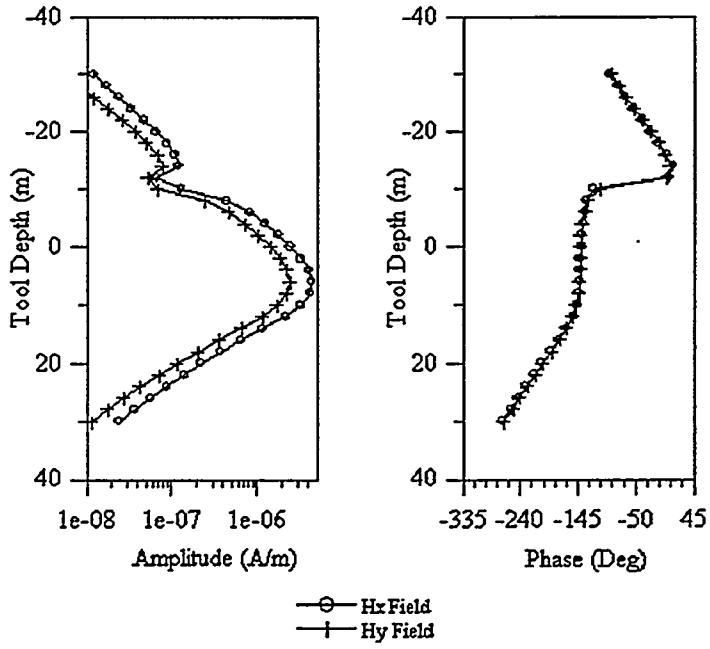

Figure 21 – Forward simulations for the model in Figure 19a comparing the Hx and Hy fields generated by a source aligned with the axis of the borehole.

SOURCE ALIGNED PERPENDICULAR TO THE BOREHOLE AXIS

In Figure 22 we have plotted the amplitudes and phases of the Hx and Hy magnetic fields that result when a horizontal magnetic dipole source oriented in the x direction (XMD) is employed to excite the medium. Measuring the Hx fields due to the XMD source as shown in Figure 22a implies we are employing the coplanar (CP) configuration. Notice that the curves in Figure 22a, at least at 10KHz, exhibit side lobes in both the amplitude and phase responses. This correlate with the sensitivity analysis which indicated that the sensitivity was larger in magnitude, and of opposite sign, in the region between the source and receiver when compared to that outside the inter-probe region. This phenomena results in sign flips in the scattered fields generated by the target, which in turn produces side lobes in the total field.

Unlike the CA results in Figure 20a, Figure 22a shows the percent amplitude and phase perturbations in the 10KHz response to be greater than that of the 100KHz response. This result can also be correlated to the sensitivity study in Chapter II as this configuration was shown to be much more sensitive to the near borehole region than the CA configuration. For instance if we examine Figure 13 and 14 we see there is very little sensitivity to regions greater than 0.5L away from the borehole. Because at 100KHz a 6m source-receiver separation has been employed, the sensitivity analysis indicates that there would be minimal response for regions greater than 3m away from the borehole. Thus at 100 KHz the target will be marginally detectable using the CP tool. However at 10KHz a source-receiver separation of 16m was employed, indicating a radius of investigation of 8m away from the borehole. This larger radius of investigation places the target well within the region of influence, with a larger target response as the result.

Examining the coplanar null couple (CPNC) results given in Figure 22b, we see that the amplitude of the null coupled fields are approximately 3% of the coplanar primary field. Note that this is a smaller value compared to the CANC configuration which yielded responses of 10%. Also, both the 10KHz and 100KHz results are of the same normalized magnitude. This was not the case for the CP results in Figure 22a. Both of these observations agree with the sensitivity analysis which showed that although the CPNC configuration exhibits greater sensitivity for larger distances away from the borehole than

the CP arrangement, it also exhibits the smallest normalized sensitivity values of any of the four basic sensor configurations.

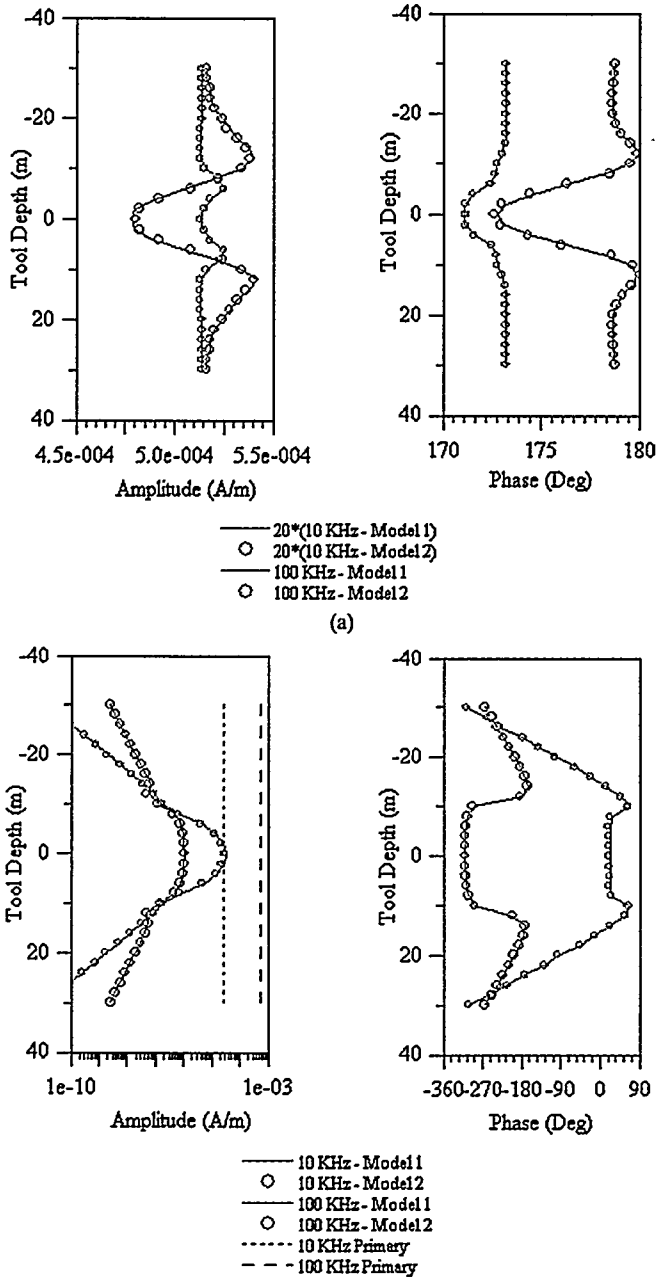

Figure 22 - Forward simulations of models shown in Figure 19 for a source aligned perpendicular to the axis of the borehole in the x direction. a) Results for coplanar configuration where both the source and receiver are aligned in the x direction perpendicular to the borehole. Note that the amplitude at 10Khz has been multiplied by 20 to fit on the same scale as the 100 KHz results. b) Results for the coplanar null coupled configuration where the field in the y direction perpendicular to the borehole axis is measured.

Finally, notice that for both of the coil configurations examined in Figure 22 the amplitude and phase responses are identical for the two models, i.e. there is no true 3D information present in either of these measurement configurations. However, the sensitivity study indicated that there is some directional information present in the CP configuration depending on the orientation of the source. This becomes apparent when we plot the Hx and Hy fields generated by horizontal magnetic dipole sources oriented in the x and y directions, respectively. These results are shown in Figure 23 where a frequency of 10KHz has been employed for the model shown in Figure 19a. Notice that the amplitude and phase are different for the two tool orientations, and thus directional information is present. However, the responses are identical if we rotate the tool(s) by 180° and thus no true 3D information is available from this measurement.

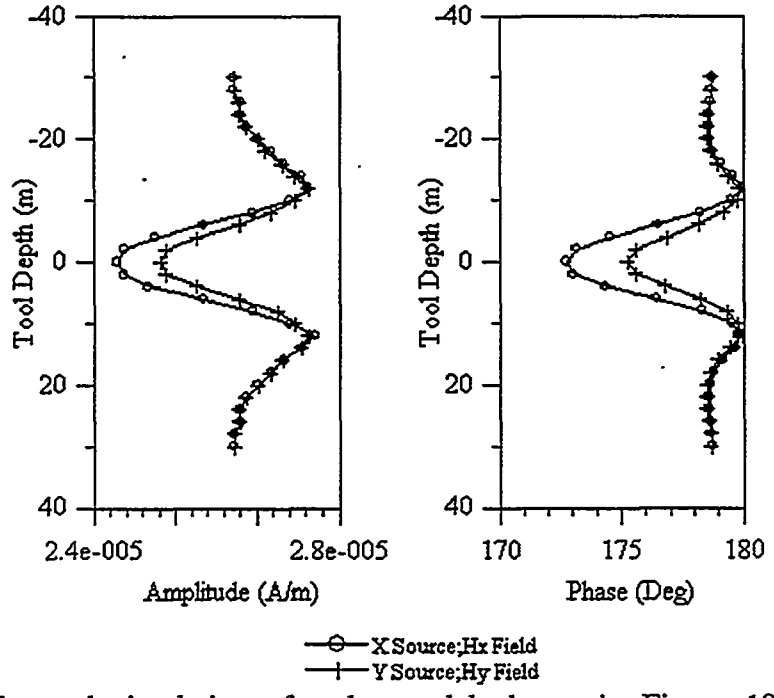

Figure 23 – Forward simulations for the model shown in Figure 19a for coplanar configurations of two different orientations.

In this section we have employed numerical modeling to validate certain elements of the sensitivity analysis presented in the previous chapter, and to demonstrate that at least for this particular target, the predicted response is well within the signal to noise limits of the proposed tool. In the case of the 10KHz measurements a source/receiver separation of

16m was employed to ensure detection at greater distances away from the borehole than normally would be achieved. Due to the technical limitations on the tool, it might be easier to employ the receiver on a separate sonde from that of the transmitter, and then connect the two by logging cable. This is especially true if we employ even larger source-receiver separations. Unfortunately this type of configuration may result in a new type of noise being introduced into the data that is caused by well deviations and/or rotation between the various sondes. Thus the assumptions about the sensor positions relative to one another would be in error. In addition, even though a tool that is built into a single sonde should be rigid enough to avoid these types of problems, as the tool becomes longer it may become susceptible to these same problems due to warping of the sonde caused by extreme downhole conditions. Thus in the next section we examine how large an error is introduced by these position errors.

ERRORS CAUSED BY TOOL MISPOSITIONING

For inversion purposes, we often assume that the data contain random Gaussian noise. However with the tool configuration shown in Figure 24a, there is the danger of corrupting the data with biased noise. As mentioned above, this bias results from assuming incorrect positions for the sources and receivers with respect to each other. Theoretically these errors could have two sources; 1) deviation of the well or warping of the tool causing the source and receiver to become misaligned (Figure 24b), and/or 2) rotation of one sensor with respect to the other (Figure 24c). Measuremetns in a real world situation will probably contain both of these types of errors (Figure 24d). In these cases, the error is introduced into the data when a given sensor becomes oriented such that it is measuring a combination of the three components of the magnetic field rather than a single component, or because the magnetic field differs between the assumed and actual measurement positions. The problem can be corrected if the position and orientation of the various tool components are tracked with respect to one another. However, the accuracy of the resulting measurements will then not only be dependent on the signal to noise characteristics of the receiver, but also on the system employed to monitor the location and orientation of the various sensors. In this section we will employ the model in Figure 19a to demonstrate how positioning errors can affect the measured

response. This will yield valuable information on how accurately we must track the relative positions of the various probes in order to recover accurate measurements of the magnetic fields.

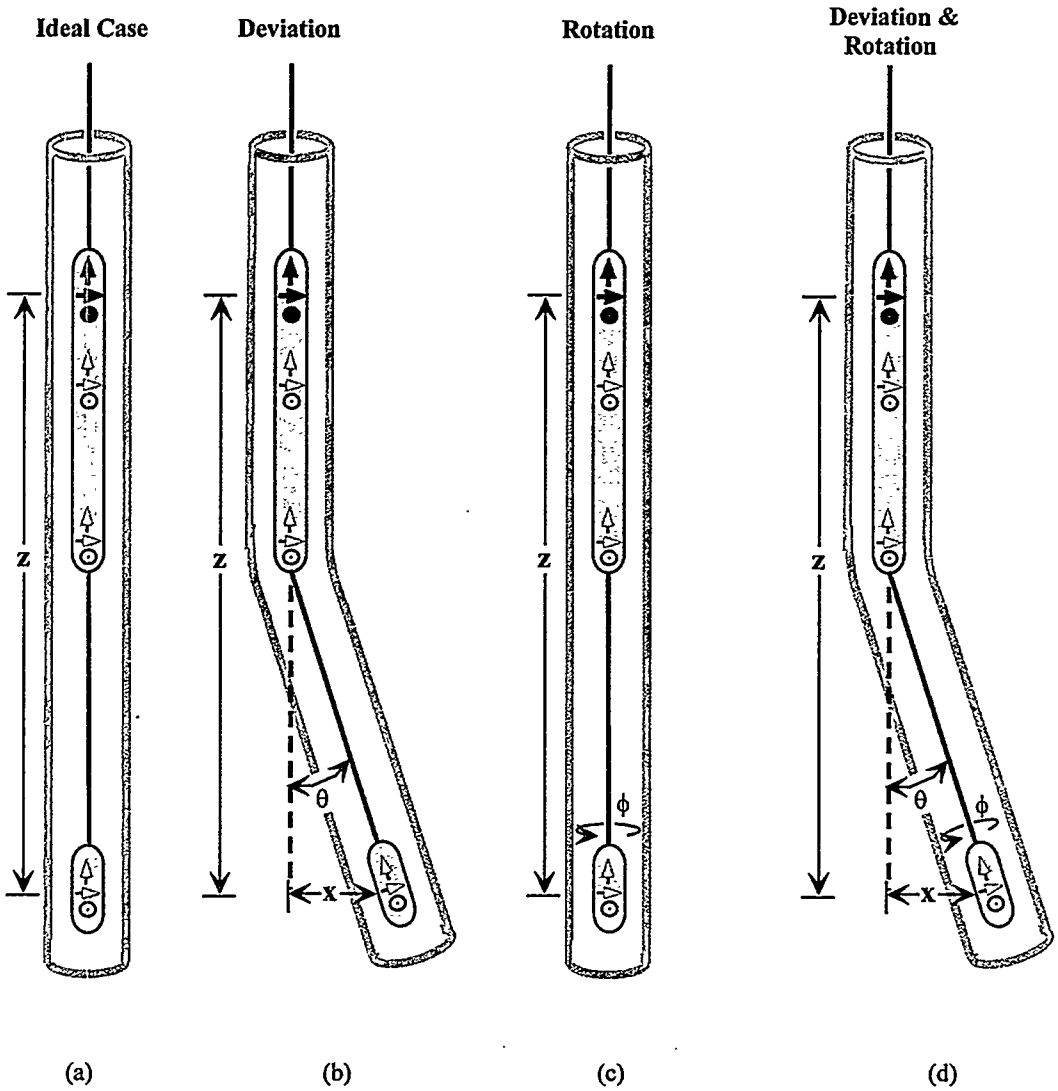

Figure 24 – Diagram of different types of orientation errors that can occur with a multiple sonde tool.

In all of the cases presented below we employ a 10 KHz frequency and a source-receiver separation of 16m. The transmitter is located 8m above the body and the receiver position starts at a depth 8m below the body and directly below the transmitter. Thus the center of the tool is located at the position where the maximum response occurs. The

receiver position is then altered to account for the different types of positioning error. In all of the cases below the fields are appropriately rotated such that the Hz' component is measured along the axis of the receiver sonde, and the Hx' and Hy' components are mutually perpendicular to each other as well as to the borehole. The results are then presented in terms of amplitude, percent amplitude error defined as $\%err = 100 * \frac{(H' - H)}{H_p}$, where H' is the deviated or rotated amplitude, H is the correct value, and H_p is the magnitude of the primary field at the correct location, and deviated or rotated phase.

DEVIATION ONLY

In Figure 25 the Hx' and Hz' fields generated by a VMD source are plotted for a receiver that has been deviated up to 5° in a direction parallel to the x axis as shown in Figure 24b. This configuration was chosen for this specific example as it was found to provide the greatest magnitude error in the Hx' component.

Notice that the maximum coupled Hz' (i.e. axial component) field has very little error associated with it. However, the errors in the Hx' (radial) field are more substantial. At 5° of deviation the amplitude error is approximately 17.5% while the phase error is nearly 100°. In fact notice that as the deviation increases, the Hx' phase converges to that of the Hz'≈ Hz phase. This helps to define the source of the biased error as the Hz field, and might provide a means of checking the radial field data to determine the magnitude of the deviation that is occurring.

Notice that to obtain a measurement to within 1% in amplitude, the deviation angle must be less than 1°, and by 2° deviation the error is almost 5%. This indicates that we must be able to track the deviation angle between the source and receiver to within 1° to obtain measurements of the desired accuracy.

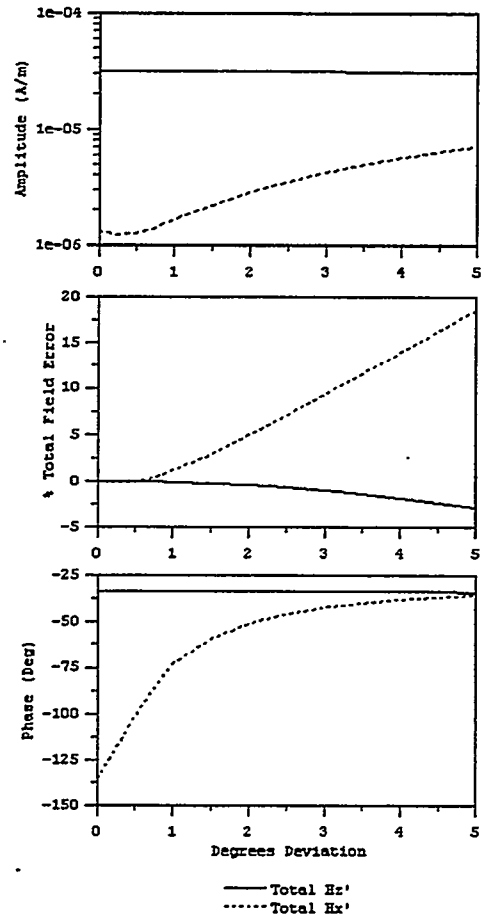

Figure 25 – Deviation error introduced in the 10KHz measurements for the model in Figure 19a and the tool center located at 0m depth. The source is aligned along the axis of the borehole, and the deviation of the receiver occurs along the x axis. The top figure is the amplitude of the rotated Hz and Hx fields, the middle figure the amplitude error in those fields as a percentage of the Hz field, and the bottom the phase of the rotated fields.

ROTATION ONLY

In Figure 26 Hx' and Hz' generated by a XMD source are plotted for a receiver that has been rotated up to 20° about the borehole axis as shown in Figure 24c. Notice that like the case presented in Figure 25 when the receiver axis was deviated compared to that of the transmitter, the maximum coupled component (i.e. the Hx' field) has very little error associated with it. Even at 20° the error is only about 6% in amplitude and less than a degree in phase. However, the Hy' component exhibits substantial errors associated with the rotation. For 20° rotation the error in amplitude is approximately 34% and phase is over 100°. Also as the angle of rotation increases, the Hy' phase converges to that of the

maximum coupled Hx phase. Thus from a simple analysis of the raw data one may be able to determine if rotation is present, and possibly even how much. Also notice that to obtain a measurement to within 1% the rotation must be less than 2°, and by 5° rotation the error is 5%. This indicates that we must be able to track the angle between the source and receiver to within 2° or so in order to obtain measurements to the desired accuracy.

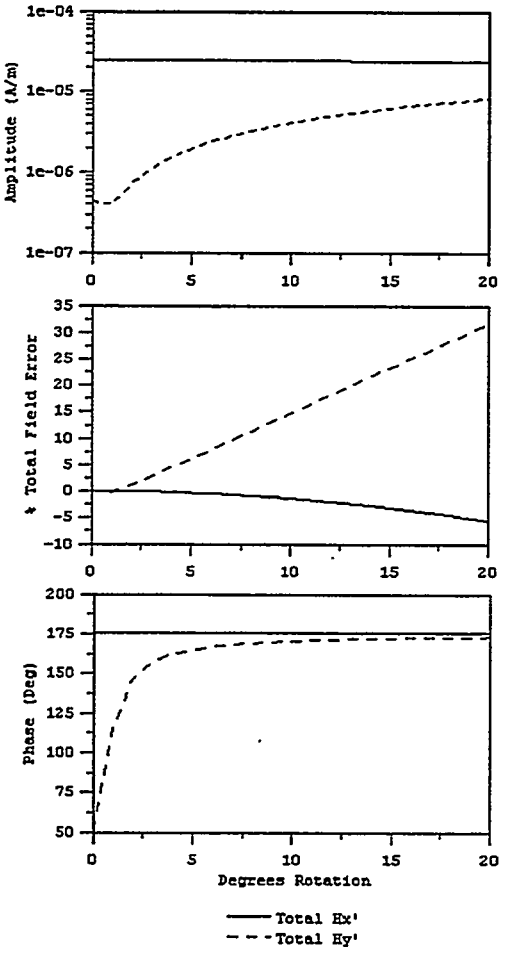

Figure 26 – Rotation error introduced in the 10KHz measurements for the model in Figure 19a and a tool position of 0m depth. The source is aligned in the x direction perpendicular to the axis of the borehole, and the rotation of the receiver occurs around the z axis. The top figure is the amplitude of the rotated Hx and Hy fields, the middle figure the amplitude error in those fields as a percentage of the Hx field, and the bottom the phase of the rotated fields.

DEVIATION AND ROTATION

As a final note we consider the case shown in Figure 24d where the tools are both deviated and rotated with respect to each other. In this particular example we assumed a VMD source aligned with the axis of the borehole, and a deviation of 5° along the x=y diagonal. The radial field errors generated by rotation about the borehole axis have been plotted in Figure 27 for rotation angles up to 20°. As one would expect, the error in the total radial fields remains constant in amplitude, such that as the amplitude error in Hy' increases, the error in Hx' decreases. In addition the phase error remains approximately constant and equal to that of the maximum-coupled field.

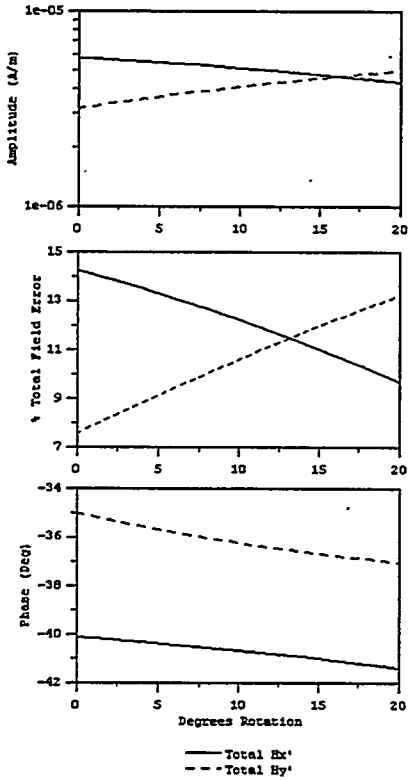

Figure 27 – Rotation and deviation error introduced in the 10KHz measurements for the model in Figure 19a and a tool position of 0m depth. The source is aligned in the z direction along the axis of the borehole, and a deviation of 5 degrees has been assumed along the x=y diagonal. The rotation of the receiver occurs around the axis of the receiver sonde. The top figure is the amplitude of the rotated Hx and Hy fields, the middle figure the amplitude error in those fields as a percentage of the Hz field, and the bottom the phase of the rotated fields.

The results given in Figures 25 through 27 indicate that a likely source of error in multi-sonde, three component induction logging measurements will be a misalignment between the source and receiver sensors. In fact this type of error could be much larger than the noise caused by the dynamic range limitations of the system. Positioning induced errors will be most prevalent in those components that are most critical in defining 3D structure of the geology surrounding the borehole, i.e. those that are perpendicular to the maximum coupled field. To account for this type of biased noise we will need to be able to track both the deviation and rotation between the source(s) and receiver(s) to within 1° to 2°. In addition, although this type of error will be almost unavoidable for a tool where the source and receivers are placed on separate sondes, single sonde arrangements may also exhibit positioning errors due to warping caused by extreme temperature and pressure conditions that exist down hole.

To this point we have established that three component measurements can probably be made within a borehole, and we have defined major sources of data error that will need to be considered as the source-receiver separation becomes larger. However we have not answered the question of how three-component magnetic field induction logging data can be interpreted, if 3D imaging of the data is possible, and if so, the resolution that will be available. In the next chapter we at least partially answer these questions with a simple inversion study that employs a synthetic data set.

CHAPTER IV

INVERSION STUDY

To test the feasibility of generating a 3D image from single borehole data in a somewhat realistic scenario, we have employed the model shown in Figure 28. In this model a horizontal well has been drilled into an oil bearing sandstone (blue) that is interbedded with lower porosity water bearing sandstones (green), shales (yellow), and a brine filled sandstone (orange). There are four main structural features within this model which we will employ to define the imaging capability of a multi-component logging tool; 1) the horizontal and vertical extent of the various formations; 2) the dip of the beds; 3) the fault located at x=0m; and 4) the 'hidden' oil zone located below the main oil reservoir in the –x half of the model. Seven frequencies spaced logarithmically from 1KHz to 100KHz were employed, and the source-receiver separations were chosen such that at each frequency an induction number (l) of either 1 or 10 was approximately maintained. Table 1 contains the separations that were employed at each frequency for the two different induction numbers.

Because of the large source-receiver separations that were employed in this simulation, the logging tool would be required to be built with multiple sondes. However due to the scaling nature of low frequency EM, the model and calculated data can be scaled for more traditional induction logging frequencies of 10KHz to 1MHz. If we increase the frequency by a factor of 10, we need to decrease the physical dimensions of the tool and the model by a factor of $\sqrt{10}$. Thus if we assume an induction number 1, the separation at 1MHZ would be approximately 1m, and at 10KHz would be 10m. This configuration would be suitable to fit on a single sonde. The appropriately scaled model in Figure 28 would then extend from ±12m in y and z, and ±26m in x. Therefore, the imaging results presented here not only hold for the scale of the long offset tool, but also to a certain extent to more traditional well logging scales.

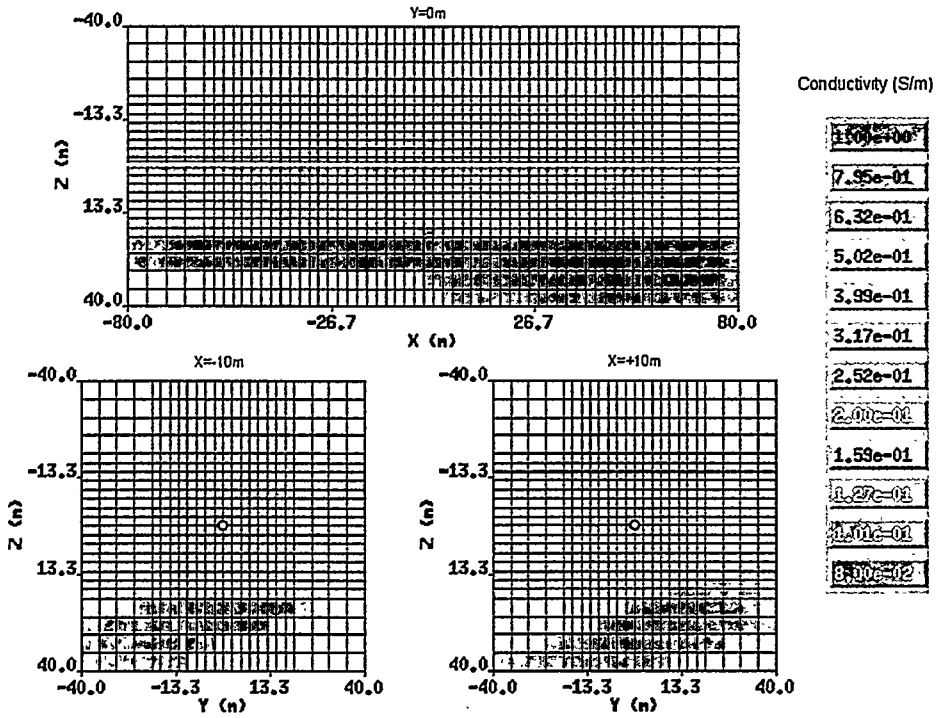

Figure 28 – Model used to investigate the possibility of 3D imaging from a single borehole. The top figure is a x-z cross section through the y=0 plane, and the bottom two figures y-z cross sections through the x=-10m and x=10m planes. The white line and circles represent the location of the borehole.

Frequency (KHz)	Source-Receiver Separation for l=1	Source-Receiver Separation for l=10
1.0	35m	110m
2.1	25m	75m
5.2	15m	50m
10	10m	35m
21	10m	25m
52	5m	15m
100	5m	10m

Table 1 – Source-receiver separations employed versus frequency for two different induction numbers.

To generate the synthetic data the 3D finite difference scheme described in Alumbaugh et al. (1996) was again employed. A measurement interval of 5m was used along the borehole for source positions starting at –100m, and receiver positions extending to +100m. Data were not calculated for sources or receivers outside this range, and thus for the longer offsets corresponding to lower frequencies there are fewer data when compared to the shorter offsets employed at higher frequencies. The modeling domain consisted of 88 cells in x, and 42 cells in both y and z, and random noise with a standard deviation equal to 1% of the primary field at each offset were added to the data. The resulting synthetic data set was then inverted using the scheme of Newman and Alumbaugh (1997) where a slightly coarser inversion (54 by 38 by 38) forward modeling mesh was employed along with an inversion domain of 48 by 32 by 32 cells. Thus we were inverting for approximately 50000 unknown conductivity values.

RESULTS FOR DIFFERENT SOURCE CONFIGURATIONS

The image that results from inverting these synthetic data using only a single polarization source oriented parallel to the axis of the borehole is shown in Figure 29. Note that with a single polarization source and 5m station spacing the data set consisted of 219 individual measurements. The run time for this inversion on Sandia's massively parallel 'Teraflop' computer was approximately 4 hours using 512 Pentium 200 MHz P2 processors with convergence occurring in 8 iterations. Notice that in general we have recovered a smoothed version of the 3D structure immediately surrounding the well. Specifically the fault has been imaged as has a portion of the primary oil zone. However, notice that the oil zone does not extend outward away from the well more than 30m. Also, it would be difficult from the image to recognize the dip in the strata. The only place the dip is discernable is in the conductive portion underlying the oil zone in the x=+10m cross section. Finally, it would be very difficult to deduce that the hidden oil zone exists from this image.

The image that results from inverting synthetic data generated from three separate sources that are orthogonally polarized is shown in Figure 30. Because the number of sources has been tripled, the total number of data points also triples to 657. The run time for

this inversion was approximately 13 hours on 512 Pentium 200 MHz P2 processors with convergence occurring in 11 iterations. Notice that we have recovered a better estimate of the 3D geology surrounding the well then we did for the single polarization source results shown in Figure 29. Specifically the oil zone is shown to extend across the entire region of interest, and the dip is much more apparent. The fault has been imaged and the conductive layer above the oil zone is better represented, although its continuity in the y direction is still pretty poor. Finally, notice that comparing the x=+10m and x=-10m cross sections that the oil zone is thicker on the right hand side of the x=-10m cross section. Thus the extra data generated with the three sources are more sensitive to the second or hidden oil when compared to the single source data. However, the resolution does not exist to image the sequence as a conductor sandwiched between two resistors, and thus is manifested as a slightly thicker resistive section both below and to the sides of the borehole. In any case, the benefit of using three orthogonal sources is evident from this example.

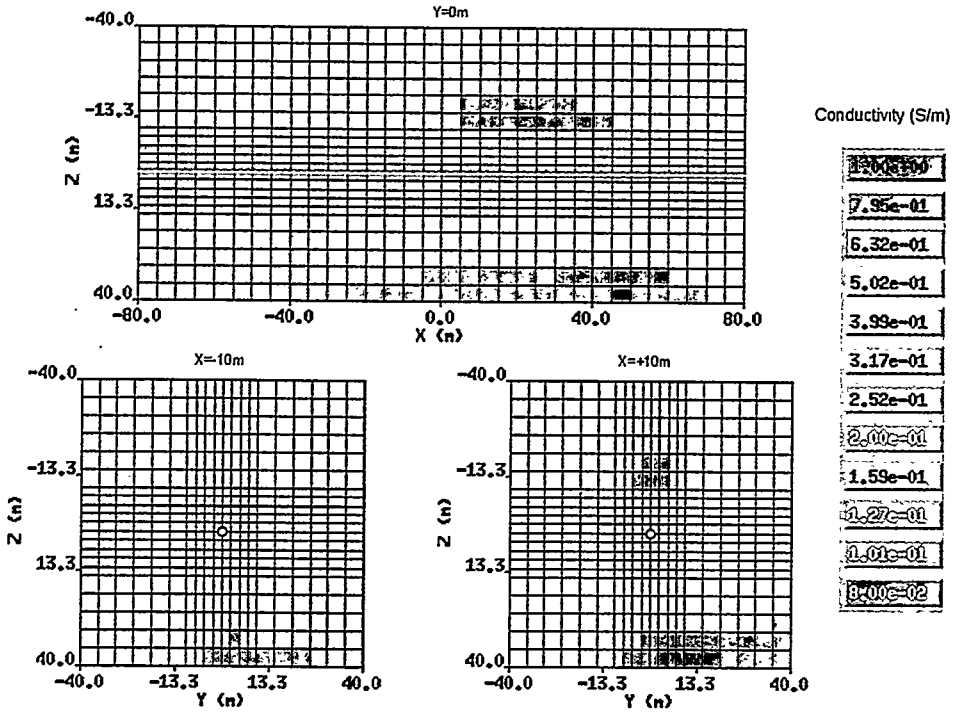

Figure 29 – Image resulting from the use of a single polarization source aligned along the axis of the borehole. An induction number of approximately 1 was employed for seven logarithmically spaced frequencies from 1KHz to 100 KHz (refer to Table 1 for the frequencies and source-receiver offsets employed). The top figure is a x-z cross section through the y=0 plane, and the bottom two figures y-z cross sections through the x=-10m and x=10m planes. The white line and circles represent the location of the borehole.

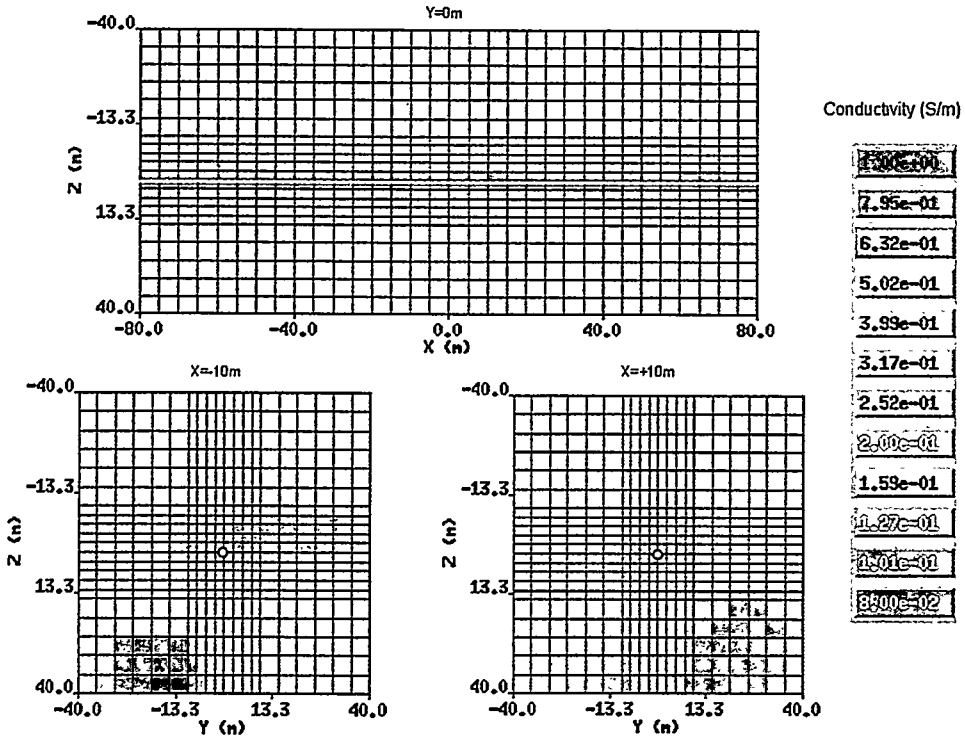

Figure 30 – Image resulting from the use of three mutually orthogonal sources at each tool position. An induction number of approximately 1 was employed for seven logarithmically spaced frequencies from 1KHz to 100 KHz (refer to Table 1 for the frequencies and source-receiver offsets employed). The top figure is a x-z cross section through the y=0 plane, and the bottom two figures y-z cross sections through the x=-10m and x=10m planes. The white line and circles represent the location of the borehole.

RESULTS FOR DIFFERENT SOURCE-RECIVER OFFSETS

In Chapter II, it was mentioned that larger source-receiver offsets should allow for sensitivity at greater distances away from the well. To illustrate this we will employ the same model, but analyze the imaging results produced by the three orthogonal sources for induction numbers of l=1 and l =10. Here using l=10 requires source-receiver separations that are three times greater than when an induction number of one is employed. In Figure 31 we have plotted a 3D view of the original model by making all cells with a conductivity greater than 0.18S/m invisible. Figure 31b is identical to Figure 31a except that it has been rotated 180° about the z axis and tilted upwards slightly. In both cases the three sides that bound the volume have been included to better illustrate the horizontal and vertical

continuity of the model. Notice that the dimensions of the model are identical to those in Figures 28 through 30, except the y axis now extends from –60m to +60m.

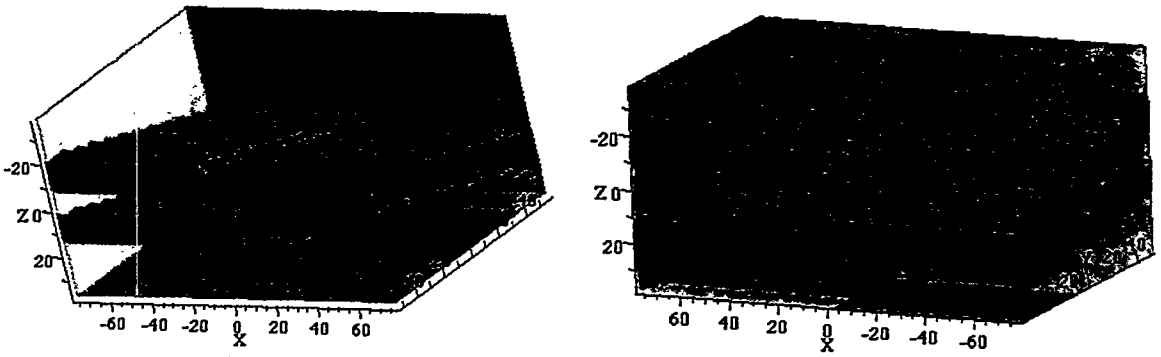

(a) (b)

Figure 31 – A 3D representation of the model shown in Figure 28. Within the volume all values greater than 0.12S/m have been made invisible. The 3 planes at x=-80m, y=-60m, and z=40m have been included to show how the rest of the model changes spatially. Figure 31b is the same as Figure 31a except it has been rotated around the z axis by 180° and tilted upwards slightly.

In Figure 32 we have plotted the inversion results for an induction number of 1, while in Figure 33 the l=10 results are rendered. As figure 32 shows, we rapidly lose sensitivity to the horizontal and vertical extent of the oil zone beyond y=±40m. Notice that the inverted results behave somewhat symmetrically about the y axis such that thicker oil zone in the –x half of the model is projected on both sides of the y axis. However as shown in Figure 33, an induction number of 10 is better able to resolve things further from the well. Notice now that in the -y half of the model the thickness of the oil zone is constant, while on the +y side, the oil becomes thicker as one progresses in the –x direction. Thus although it is not resolving the two individual oil zones, the image does yield valuable information indicating that the structure is different across the y=0 plane. This demonstrates from an imaging perspective that larger source-receiver offsets result in sensitivity at greater depths away from the well than can be achieved with shorter offsets.

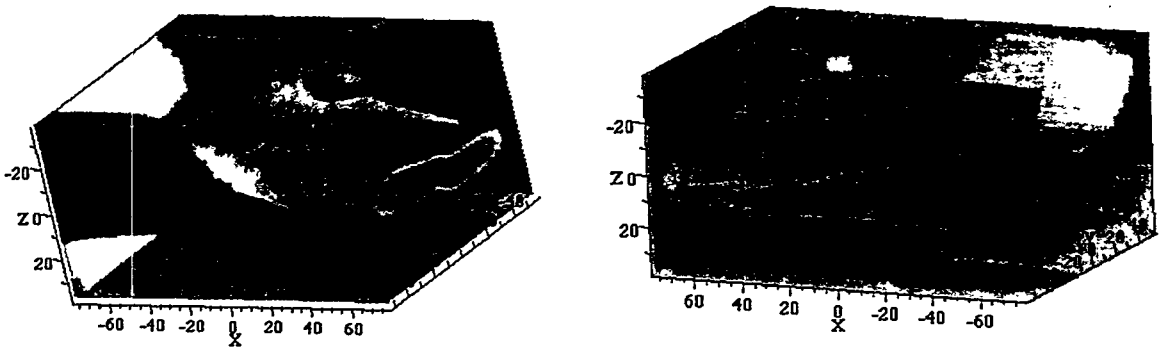

(a) (b)

Figure 32 – A 3D representation of the reconstructed model for a three polarization source and an induction number of 1 (refer to Table 1 for the frequencies and source-receiver offsets employed). Within the volume all values greater than 0.12S/m have been made invisible. The 3 planes at x=-80m, y=-60m, and z=40m have been included to show how the rest of the model changes spatially. Figure 32b is the same as Figure 32a except it has been rotated around the z axis by 180° and tilted upwards slightly.

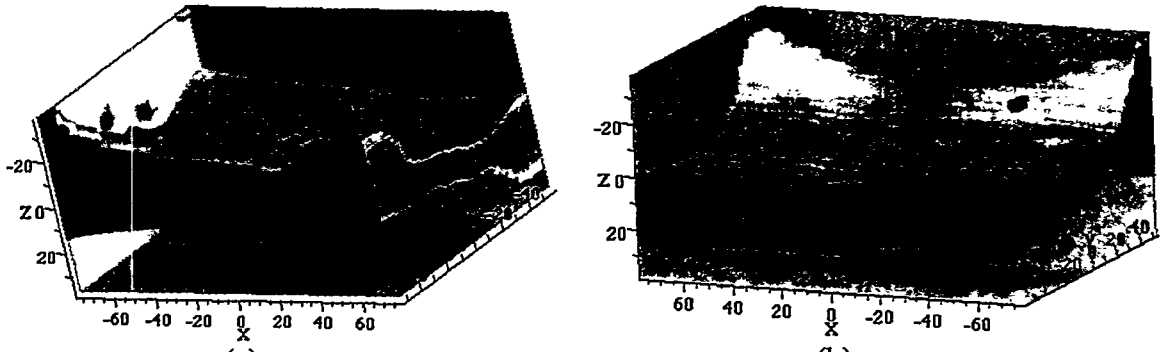

(a) (b)

Figure 33 – A 3D representation of the reconstructed model for a three polarization source and an induction number of 10 (refer to Table 1 for the frequencies and source-receiver offsets employed). Within the volume all values greater than 0.12S/m have been made invisible. The 3 planes at x=-80m, y=-60m, and z=40m have been included to show how the rest of the model changes spatially. Figure 33b is the same as Figure 33a except it has been rotated around the z axis by 180° and tilted upwards slightly.

CHAPTER V

CONCLUSIONS AND DISCUSSION

In this paper we have demonstrated the plausibility of multi component induction logging to delineate 3D structure in the region surrounding a borehole. To do this we have employed theoretical sensitivity calculations, forward modeling, and 3D inversion on synthetic test data. The analysis has demonstrated the specific tool configurations and frequencies that should be employed to generate 3D images from total field - induction logging data collected by a multiple sonde tool in a single borehole. For example it has been determined that as great a transmitter-receiver separation should be employed as feasibly possible up to 70m or so, along with a low enough frequency such that the induction number is less than 10. Above this value the signal to noise characteristics of the measurements rapidly degrades. However, due to the presence of the primary or whole space field, the signal to noise characteristics will also degrade as the induction number is decreased below a value of 0.1. In addition, attempting to make measurements at lower induction numbers than this will not provide greater sensitivity depths. Thus in order to provide the resolution of the scattered fields while also providing maximum depth sensitivity away from the well, we suggest operating in the induction number range of 0.1 to 10.

In terms of the various tool configurations, the CA configuration in Figure 2a offers the best signal to noise characteristics, and the greatest depth of sensitivity away from the borehole of any of the tool configurations. It is no coincidence that this configuration is the standard employed by the oil service industry. However, because the sensitivity is symmetric about the borehole, no 3D information is provided by this arrangement.

The CANC configuration shown in Figure 2b is the only source-receiver configuration that provides true 3D information. To provide a full 3D scan around the borehole, two receivers (or sources) oriented perpendicular to both the borehole axis and each other must be coupled with an axially aligned source (or receiver). Unfortunately, the depth of sensitivity away from the borehole is limited for this tool when compared the CA configuration. Thus as large a separation as possible must be employed to achieve full 3D sensitivity at great distances away from the borehole.

The CP tool configuration (Figure 2c) also demonstrates a limited depth of sensitivity away from the borehole. In addition, although it does provide some directional information, it does not provide full 3D sensitivity. However, due to the fact that the sensitivity changes sign on opposite sides of the source/receiver as one moves along the borehole axis, this tool will provide excellent resolution in the direction along the borehole.

The CPNC system offers excellent directional sensitivity, although it too does not offer true 3D information. However when coupled with the CANC tool it should greatly enhance the horizontal resolution due to the fact that the response is zero where the CANC system maximizes, and vice versa. Also, this configuration exhibits better sensitivity with depth away from borehole than any other arrangement outside of the CA tool. However, it also exhibits poorest signal to noise characteristics of any of the configurations.

It has been demonstrated numerically that the null coupled components so important to the reconstruction of a 3D image are comparable in magnitude to the scattered maximum coupled fields, and thus are easily measured within the signal to noise limitations of the logging tool. However, these null coupled components are very susceptible to biased errors caused by misalignment between the source and receiver, and thus a careful determination of the relative positions and orientations of the sensors is required. Finally it has been demonstrated that 3D images can be reconstructed from single borehole measurements, and that image resolution improves by measuring data generated by three separate and orthogonal sources, and by employing as large a source-receiver offset as possible.

One drawback of the method is that inversion modeling was completed using a massively parallel computer available at Sandia National Laboratories. Thus at present powerful computers are required that may not be available to many geophysicists in order to process this type of data using a full nonlinear inversion scheme. However, with the rapid increase in computational speed coupled with decreasing cost of CPU's this may not be a major issue in the future.

One thing that has not been fully addressed is the magnitude of the borehole reflections on the measurements, especially when the CP configuration is employed. Numerical modeling has shown that reflections develop which can dominate the response

for these source geomtries (K. M. Strack, A. Tripp, 1998, Personal Communication). In addition, the effects of formation anisotropy have been ignored in this study. This phenomenon can severely alter the logging response in horizontal wells. Thus in the near future we will begin to examine these phenomena, and determine how much they affect the measurements and resulting images. In addition we hope to develop appropriate methods for dealing with them.

REFERENCES

Alumbaugh, D.L., Newman, G.A., Prevost, L., and Shadid, J.N., 1996, Three-dimensional wide band electromagnetic modeling on massively parallel computers: Radio Science , **31**, 1-23.

Anderson, B., 1986, The analysis of some unsolved induction interpretation problems using computer modeling; The Log Analyst, **27**, (5), 60-73.

Doll, H. G., 1949, Introduction to induction logging and application to logging of wells drilled with oil base mud; Journal of Petroleum Technology, 148-162.

Gianzero, S., and Anderson, B., 1982, A new look at skin effect; The Log Analyst, **23**, (1), 20-34.

Hohmann, G. W., 1975, Three-dimensional induced polarization and electromagnetic modeling; Geophysics, **40**, 309-324.

Kong, J. A., 1975, Theory of Electromagnetic Waves, John Wiley and Sons, New York.

Moran, J. H., 1982, Induction logging – geometrical factors with skin effect; The Log Analyst, **23**, (6), 4-10.

Newman, G.A., and Alumbaugh, D.L., 1997, Three-dimensional massively parallel inversion - I. Theory; Geophys. J. Int., **128**, 345-354.

Sato, T., Osato, K., Takasugi, S., and Uchida, T., 1996, Development of the Multi-Frequency Array Induction Logging (MAIL) Tool; Geothermal Resources Council Transactions, **20**, 637-642.

Spies, B. R. , and Habashy, T. M., 1995, Sensitivity analysis of crosswell electromagnetics; Geophysics, **60**, 834-845.

Ward, S. H., and Hohmann, G. W., Electromagnetic theory for geophysical applications; *in* M. N. Nabighian, ed., Electromagnetic Methods in Applied Geophysics – Theory, Vol. 1: Soc. Explor. Geophys., 131-311.

Wilt, M.J., and Alumbaugh, D.L., 1998, Electromagnetic methods for development and production; state of the art: The Leading Edge, **17**, 487-492.

APPENDIX A

To derive the sensitivities, we employ a method similar to that of Spies and Habashy (1995). If we assume that we are operating in a whole space of isotropic conductivity with scattering inclusions, the derivation starts with the vector integral equation for the magnetic fields such as given in Hohmann (1975);

$$\mathbf{H}(x,y,z) = \mathbf{H}^{\mathrm{p}}(x,y,z) + \int (\sigma_b - \sigma(x',y',z'))\tilde{\mathbf{G}}^{\mathbf{H}}(x,y,z;x'y'z')\mathbf{E}(x',y',z')dv' . \qquad \text{(A1)}$$

Here $\mathbf{H}(x,y,z)$ represents the total magnetic field at point (x,y,z), $\mathbf{H}^{\mathrm{p}}(x,y,z)$ is the primary or whole space field that would exist at the receiver in the absence of any inhomogeneities, $\mathbf{E}(x',y',z')$ represents the total electric field at the point (x',y',z') within the medium, $\sigma(x',y',z')$ is the electrical conductivity at that point, and σ_b represents the background electrical conductivity of the homogenous medium. $\tilde{\mathbf{G}}^{\mathbf{H}}(x,y,z;x',y',z')$ is the tensor Green's function for a whole space which relates the electric scattering current at (x',y',z') to the magnetic field at (x,y,z). Note, this expression assumes the source is located at (0,0,0).

Notice that the term underneath the integral in Equation (A1) represents the scattered magnetic field generated by scattering currents, and that the equation is nonlinear in conductivity because the electric field is dependent on this property. However, we can linearize this expression by applying the Born Approximation (Kong, 1975) which replaces the total electric field ($\mathbf{E}(x',y',z')$) in the medium with the primary, or whole space background electric field produced by the transmitter ($\mathbf{E}^{\mathrm{p}}(x',y',z')$), i.e.;

$$\mathbf{H}(x,y,z) \approx \mathbf{H}^{\mathrm{p}}(x,y,z) + \int (\sigma_b - \sigma(x',y',z'))\tilde{\mathbf{G}}^{\mathbf{H}}(x,y,z;x'y'z')\mathbf{E}^{\mathrm{p}}(x',y',z')dv' . \qquad \text{(A2)}$$

Notice that now the expression is linear between $\mathbf{H}$ and σ. Because we can analytically calculate $\tilde{\mathbf{G}}^{\mathbf{H}}(x,y,z;x'y'z')$ and $\mathbf{E}^{\mathrm{p}}(x',y',z')$ for a whole space, we can set up an inverse equation to estimate the unknown conductivity distribution. Note the quality of that estimate will depend on the number and quality of data ($\mathbf{H}$) that we collect. Notice also that the product $\tilde{\mathbf{G}}^{\mathbf{H}}(x,y,z;x'y'z')\ \mathbf{E}^{\mathrm{p}}(x',y',z')$ underneath the integral sign relates perturbations in the model (σ_b - $\sigma(x',y',z')$) to perturbations in the magnetic field, i.e. this represents the sensitivity ($\mathbf{S}(x,y,z;x',y',z')$) of the data to the model. Thus if we plot this product as a

function of location and/or frequency, we can determine to which regions a given source/receiver combination are most sensitive. This is the method used by Moran (1982) to derive the response functions for standard induction tools.

As previously mentioned, $\tilde{\mathbf{G}}^{\mathrm{H}}(x,y,z;x'y'z')$ is a tensor which is explicitly written as

$$\tilde{\mathbf{G}}^{\mathrm{H}} = \begin{bmatrix} G_{xx}^H & G_{xy}^H & G_{xz}^H \\ G_{yx}^H & G_{yy}^H & G_{zy}^H \\ G_{zx}^H & G_{zy}^H & G_{zz}^H \end{bmatrix}. \tag{A3}$$

The first subscript represents that component of the magnetic field that is being measured at the receiver point (*x,y,z*), and the second subscript the component of the electric field within the medium which is causing the scattering at the location (*x',y',z'*). Because the electric field, $\mathbf{E}^{\mathrm{P}}(x',y',z')$, is a vector, the sensitivity can be written in component form as

$$\begin{aligned} \mathbf{S}(x,y,z;x'y'z') = (G_{xx}^H E_x^P + G_{xy}^H E_y^P + G_{xz}^H E_z^P)\hat{\mathbf{i}} \\ +(G_{yx}^H E_x^P + G_{yy}^H E_y^P + G_{yz}^H E_z^P)\hat{\mathbf{j}} \\ +(G_{zx}^H E_x^P + G_{zy}^H E_y^P + G_{zz}^H E_z^P)\hat{\mathbf{k}} \end{aligned} \tag{A4}$$

where E_x^P, E_y^P and E_z^P are the x, y, and z components of the primary electric field generated at point (*x',y',z'*) by an arbitrarily oriented magnetic dipole source located at (0,0,0), and the $\hat{\mathbf{i}}$, $\hat{\mathbf{j}}$, and $\hat{\mathbf{k}}$ represent unit vectors of the sensitivity for the field measured in the x,y, and z directions, respectively.

The nine components of the tensor given in Equation (A3) can be derived from expressions in Ward and Hohmann (1987) as;

$$\begin{aligned} G_{xx}^H &= G_{yy}^H = G_{zz}^H = 0, \\ G_{yx}^H &= -F(x,y,z;x',y',z')\frac{(z-z')}{r}\hat{\mathbf{j}}, \\ G_{zx}^H &= F(x,y,z;x',y',z')\frac{(y-y')}{r}\hat{\mathbf{k}} \\ G_{xy}^H &= F(x,y,z;x',y',z')\frac{(z-z')}{r}\hat{\mathbf{i}}, \\ G_{zy}^H &= -F(x,y,z;x',y',z')\frac{(x-x')}{r}\hat{\mathbf{k}} \end{aligned} \tag{A5}$$

$$G_{xz}^{H} = -F(x,y,z;x',y',z')\frac{(y-y')}{r}\hat{\mathbf{i}},$$

$$G_{yz}^{H} = F(x,y,z;x',y',z')\frac{(x-x')}{r}\hat{\mathbf{j}}$$

where

$$F(x,y,z;x',y',z') = \frac{(ikr+1)}{4\pi r^2}e^{-ikr} \qquad \text{(A6)}$$

and $r = \sqrt{(x-x')^2 + (y-y')^2 + (z-z')^2}$. In expression (A6), k is the wave number for the whole space background which for the quasi static case examined here is defined by $k = \sqrt{-i\omega\mu\sigma}$. In this expression ω is the angular frequency, $i = \sqrt{-1}$ and μ is the magnetic permeability of free space which has a value of $4\pi X10^{-7}$ Henry/m.

For the vertical magnetic dipole source shown in Figures 2a and 2b, the primary electric field has components in the x and y directions are given as

$$E_x^P = -i\omega\mu mF(x',y',z';0,0,0)\frac{(y')}{r}\hat{\mathbf{i}},$$

$$E_y^P = i\omega\mu mF(x',y',z';0,0,0)\frac{(x')}{r}\hat{\mathbf{j}} \qquad \text{(A7)}$$

where m is the magnetic dipole moment of the transmitter. Similarly we can write the electric field components for the horizontal x directed magnetic dipole sources employed for the configurations shown in Figures 2c and 2d as

$$E_y^P = -i\omega\mu mF(x',y',z';0,0,0)\frac{(z')}{r}\hat{\mathbf{j}},$$

$$E_z^P = i\omega\mu mF(x',y',z';0,0,0)\frac{(y')}{r}\hat{\mathbf{k}}. \qquad \text{(A8)}$$

Now that we have written out the various components in Expressions (A4) through (A8) we can write the sensitivity for each of the configurations shown in Figure 2. Assuming a receiver location of x=0,y=0,z=l, the sensitivity for the CA configuration in Figure 2a is given by

$$S^{CA}(0,0,l;x'y'z') = (G^H_{xx}E^P_x + G^H_{xy}E^P_y)\hat{\mathbf{k}} =$$

$$i\omega\mu mF(0,0,l;x',y',z')F(x',y',z';0,0,0)\left(\frac{y'}{r}\right)^2 \qquad \text{(A9)}$$

$$+i\omega\mu mF(x,y,z;x',y',z')F(x',y',z';0,0,0)\left(\frac{x'}{r}\right)^2,$$

while for the CANC tool illustrated in Figure 2b, S is given as

$$S^{CANC}(0,0,l;x'y'z') = G^H_{xy}E^P_y\hat{\mathbf{i}} =$$

$$-i\omega\mu mF(0,0,l;x',y',z')F(x',y',z';0,0,0)\frac{x'z'}{r^2}. \qquad \text{(A10)}$$

Similarly for the CP and CPNC configurations shown in Figure 2c and 2d, respectively, the sensitivities are given as

$$S^{CP}(0,0,l;x'y'z') = (G^H_{xy}E^P_y + G^H_{xz}E^P_z)\hat{\mathbf{i}} =$$

$$i\omega\mu mF(0,0,l;x',y',z')F(x',y',z';0,0,0)\left(\frac{z'}{r}\right)^2 \qquad \text{(A11)}$$

$$+i\omega\mu mF(x,y,z;x',y',z')F(x',y',z';0,0,0)\left(\frac{y'}{r}\right)^2$$

and

$$S^{CPNC}(0,0,l;x'y'z') = G^H_{yz}E^P_z\hat{\mathbf{i}} =$$

$$-i\omega\mu mF(0,0,l;x',y',z')F(x',y',z';0,0,0)\frac{x'z'}{r^2}. \qquad \text{(A12)}$$

Distribution

David Alumbaugh
University of Wisconsin-Madison
2258 Engineering Hall
1415 Engineering Drive
Madison, WI 53706

Mike Wilt
Electromagnetic Instruments, Inc.
1301 South 46th Street, Bldg. 300
Richmond Field Station
University of California
Richmond, CA 94804

Frank Morrison
Electromagnetic Instruments, Inc.
1301 South 46th Street, Bldg. 300
Richmond Field Station
University of California
Richmond, CA 94804

Ed Nichols
Electromagnetic Instruments, Inc.
1301 South 46th Street, Bldg. 300
Richmond Field Station
University of California
Richmond, CA 94804

Ki Ha Lee
Lawrence Berkeley Laboratory
Bldg. 90-1116
1 Cyclotron Road
Berkeley, CA 94720

Mike Hoversten
Lawrence Berkeley Laboratory
Bldg. 90-1116
1 Cyclotron Road
Berkeley, CA 94720

Marshall Reed
U.S. Department of Energy
Office of Geothermal Technologies
EE-12, MS 6A-116
Forrestal Bldg.
1000 Independence Ave. SW
Washington, DC 20585

David Aldridge, 6116 MS-0750
Lewis Bartel, 6116, MS-0750
David Borns, 6116 MS-0750
Thurlow Caffey, 6116 MS-0750
Gregory Newman, 6116 MS-0750
Neill Symons, 6116 MS-0750
Marianne Walck, 6116 MS-0750
Chester Weiss, 6116 MS-0750

Central Technical Files, 8940-2 MS-9018
Technical Library, 4916 MS-0899
Review & Approval Desk, 4912 MS-0612
For DOE/OSTI